scientific reports

Check for updates

OPEN

Non-electrophilic NRF2 activators promote wound healing in human keratinocytes and diabetic mice and demonstrate selective downstream gene targeting

May Barakat[1,2], Chen Han[1,2], Lin Chen[1], Brian P. David[3], Junhe Shi[1,5], Angela Xu[1], Kornelia J. Skowron[3], Tatum Johnson[3], Reginald A. Woods[1,2], Aparna Ankireddy[4], Sekhar P. Reddy[4,6], Terry W. Moore[3,6]✉ & Luisa A. DiPietro[1]✉

The transcription factor NRF2 plays an important role in many biological processes and is a promising therapeutic target for many disease states. NRF2 is highly expressed in the skin and is known to play a critical role in diabetic wound healing, a serious disease process for which treatment options are limited. However, many existing NRF2 activators display off-target effects due to their electrophilic mechanism, underscoring the need for alternative approaches. In this work, we investigated two recently described non-electrophilic NRF2 activators, ADJ-310 and PRL-295, and demonstrated their efficacy in vitro and in vivo in human keratinocytes and *Lepr*$^{db/db}$ diabetic mice. We also compared the downstream targets of PRL-295 to those of the widely used electrophilic NRF2 activator CDDO-Me by RNA sequencing. Both ADJ-310 and PRL-295 maintained human keratinocyte cell viability at increasing concentrations and maintained or improved cell proliferation over time. Both compounds also increased cell migration, improving in vitro wound closure. ADJ-310 and PRL-295 enhanced the oxidative stress response in vitro, and RNA-sequencing data showed that PRL-295 activated NRF2 with a narrower transcriptomic effect than CDDO-Me. In vivo, both ADJ-310 and PRL-295 improved wound healing in *Lepr*$^{db/db}$ diabetic mice and upregulated known downstream NRF2 target genes in treated tissue. These results highlight the non-electrophilic compounds ADJ-310 and PRL-295 as effective, innovative tools for investigating the function of NRF2. These compounds directly address the need for alternative NRF2 activators and offer a new approach to studying the role of NRF2 in human disease and its potential as a therapeutic across multiple disease states.

Keywords Nuclear factor erythroid 2 related factor 2, NRF2 activation, Keratinocyte, Oxidative stress, Diabetic wound healing

Abbreviations

AKR	Aldo-keto reductase
ANOVA	Analysis of variance
CDDO-Me	Bardoxolone-methyl
SOD	Superoxide dismutase
D	Day
DEG	Differentially expressed gene
DFU	Diabetic foot ulcer
DMEM	Dulbecco's Modified Eagle Medium

[1]Center for Wound Healing and Tissue Regeneration, University of Illinois Chicago College of Dentistry, Chicago, IL, USA. [2]Medical Scientist Training Program, University of Illinois Chicago College of Medicine, Chicago, IL, USA. [3]Department of Pharmaceutical Sciences, University of Illinois Chicago College of Pharmacy, Chicago, IL, USA. [4]Department of Pediatrics, University of Illinois Chicago College of Medicine, Chicago, IL, USA. [5]Institute of Clinical Pharmacology, Xiyuan Hospital, China Academy of Chinese Medical Sciences, Beijing, China. [6]University of Illinois Cancer Center, Chicago, IL, USA. ✉email: twmoore@uic.edu; ldipiet@uic.edu

DO	Human Disease Ontology
FDR	False discovery rate
GCLC	Glutamate-cysteine ligase catalytic subunit
GCLM	Glutamate-cysteine ligase modifier subunit
GO	Gene Ontology
GSH	Glutathione
GST	Glutathione S-transferase
H or h	Hours
HaCaT	Human immortalized keratinocyte
HEPES	N-2-hydroxyethylpiperazine-N'-2-ethanesulfonic acid
HMOX 1	Heme oxygenase 1
KEGG	Kyoto Encyclopedia of Genes and Genomes
MTS	CellTiter 96 AQueous One Solution Cell Proliferation Assay
NFE2L2	Nuclear factor erythroid 2 related factor 2
NIH	National Institutes of Health
NQO1	NADPH quinone dehydrogenase 1
NRF2	NFE2L2, nuclear factor erythroid 2 related factor 2
PCR	Polymerase chain reaction
PG	Pluronic gel
Reactome	Reactome Pathway Database
RT-PCR	Real Time PCR
ROS	Reactive oxygen species
SD	Standard deviation
SEM	Standard error of the mean
CRediT	Contributor Roles Taxonomy

Since the 1850s, scientists and physicians have described the phenomenon of chronic wounds in patients with diabetes[1]. In the 150 + years that have passed since, the management and treatment of diabetes mellitus (DM) have improved exponentially, but despite this progress in targeting the disease itself, there are few effective treatment options for the management of chronic diabetic foot ulcers (DFUs), a common and life-threatening complication for diabetic patients[2]. A significant body of work has sought to identify potential therapeutic targets for DFUs[2]. One such target is the transcription factor nuclear factor erythroid 2-related factor 2 (NFE2L2, also known as NRF2).

First isolated in 1994, NRF2 is a basic leucine zipper protein in the cap'n'collar family that controls an important cytoprotective pathway[3–7]. Although its most well-known functions lie in mitigating oxidative damage by regulating key players in oxidative stress response and toxicity, NRF2 plays a role in many cellular processes, including homeostasis, inflammation, and metabolism; it also regulates the expression of hundreds of downstream genes, including heme oxygenase 1 (HMOX1), glutamate-cysteine ligase catalytic and modifier subunits (GCLC, GCLM), NADPH quinone dehydrogenase 1 (NQO1), superoxide dismutases (SODs), glutathione S-transferases (GSTs), aldo-keto reductases (AKRs), and many more[4,6–27].

NRF2 has been implicated both positively and negatively in several disease states, including a multitude of cancers, neurodegenerative disorders, lung diseases, gastrointestinal and hepatic diseases, chronic kidney disease, diabetic nephropathy, rheumatoid arthritis, autoimmune conditions, and more[28–30]. Due to its broad array of effects, NRF2 is often considered a widespread "protector" of organs and tissues, and pharmacologic activation of NRF2 is an area of considerable interest across these conditions[13,28,31]. These investigations are not without their challenges, however, most notably owing to the variability in NRF2 effects depending on the disease context. NRF2 activation has demonstrated both anti-cancer and pro-carcinogenic effects at different stages of cancer development[28], highlighting both the complexity of antioxidant and immune responses and the need for a detailed understanding and characterization of NRF2 activators that may progress to clinical use[31].

In the context of diabetes, NRF2 has been shown to play a critical role in diabetic wound healing[32]. In human patients, diabetic skin exhibits increased oxidative stress and decreased NRF2 expression[33]. Diabetic *NRF2*$^{-/-}$ knockout mice heal more slowly than diabetic *NRF2*$^{+/+}$ mice do, and exogenous NRF2 activation improves wound healing in diabetic mice but not in wild-type mice[32–35]. Furthermore, pharmacologic inhibition or knockdown of NRF2 delays wound healing and exacerbates diabetes-induced oxidative stress[36]. These findings underscore the potential role of NRF2 in the treatment and prevention of diabetic wounds, garnering widespread interest in investigating the roles, mechanisms, and mediators of the NRF2 pathway in diabetic wound healing[37–39]. In addition to direct wound healing applications, NRF2 targeting has also been studied to address the upstream cardiovascular complications of diabetes, including severe sequelae such as stroke, diabetic retinopathy, and heart failure[40].

Several existing NRF2 activators have been investigated as potential therapeutics for diabetic wounds and other conditions, including kidney disorders, Alport syndrome, multiple cancers, lung disease, autoimmune diseases, and many others[28,41,42]. These compounds include bardoxolone methyl, omaveloxolone, dimethyl fumarate, sulforaphane, curcumin, and resveratrol[41]. In particular, bardoxolone methyl (CDDO-Me), also known as RTA-402, is among the most well-known and thoroughly studied agents due in large part to several clinical trials investigating its efficacy in treating diabetes, obesity, chronic kidney disease, diabetic and IgA nephropathy, and liver and gallbladder diseases[28,41,43,44]. CDDO-Me has previously been shown to have significant anti-diabetic effects on diabetic *Lepr*$^{db/db}$ mice[45]. More recently, the NRF2-activating effects of the bardoxolone family have been investigated for their potential in managing COVID-19 infection[46,47]. Among these existing NRF2 activators, few are currently used clinically, and several other clinical trials employing NRF2

activators are still ongoing[31]. As of June 2023, there are three NRF2-activating drugs approved by the FDA: Tecfidera (dimethyl fumarate) and Vumerity (diroximel fumarate), which are used for the treatment of relapsing and remitting multiple sclerosis, and Skyclarys (omaveloxolone), which was approved in March 2023 and is the only available treatment for Friedrich's ataxia.

The majority of pre-existing NRF2 activators are electrophilic molecules that activate NRF2 by covalently binding its cytoplasmic regulatory protein, Kelch-like ECH-associated protein 1 (KEAP1), which, along with Cullin-3, sequesters NRF2 in the cytoplasm and tags it for degradation through the ubiquitin–proteasome pathway[31,41,48–50]. Electrophilic compounds may demonstrate substantial off-target effects, and proteomics studies have shown that compounds such as CDDO-Me interact with hundreds of targets[31,51–53]. A promising alternative mechanism of NRF2 activation involves directly blocking the protein–protein interaction between NRF2 and KEAP1[41]. To this end, our research groups have previously developed two non-electrophilic NRF2 activators, PRL-295 and ADJ-310 (Fig. 1)[54,55]. PRL-295 provides support for the proposed Hinge-and-Latch mechanism of NRF2 activation and has previously been shown to directly interact with KEAP1 in cells[50,56]. PRL-295-mediated induction of downstream target genes is absent in NRF2 knockout mice, confirming that PRL-295 directly activates NRF2 by binding with KEAP1[56].

The present study examined the effects of PRL-295 and ADJ-310 in in vitro and in vivo models of wound healing and analyzed NRF2-associated mechanisms involved in wound repair. To understand the effects of these non-electrophilic small molecules in vitro, human keratinocytes (HaCaT cells) were treated with 1, 5, or 10 µM ADJ-310 or PRL-295. Cell viability, proliferation, in vitro wound closure, and antioxidant activity were assessed. Additionally, HaCaT cells treated with PRL-295 or CDDO-Me were subjected to mRNA sequencing to compare the expression of their downstream targets and to examine the pathways involved in the response to treatment. To investigate the effects of these compounds on diabetic wound healing in vivo, full-thickness excisional skin wounds were created on the backs of diabetic *Lepr*$^{db/db}$ mice and treated daily with 100 µg of each compound. Wound healing was measured daily, and additional treated wounds were harvested for RT-PCR analysis.

Results

ADJ-310 and PRL-295 promote wound healing functions in human keratinocytes

To determine the effects of the non-electrophilic NRF2 activators ADJ-310 and PRL-295 on wound healing in vitro, we first examined their impact on cell viability (Fig. 2). Human keratinocytes (HaCaT cells) were selected because keratinocytes represent the majority of the cells in the healing wound and exhibit high NRF2 expression and activity[18,57]. HaCaT cells were cultured to confluence and then treated with DMEM containing 1, 5, or 10 µM ADJ-310 or PRL-295 for 24 h. Negative control cells were treated with DMEM containing 10 µL/mL (1%) DMSO, and positive control cells were treated with DMEM containing 250 nM CDDO-Me. This concentration was selected for positive control cells based on a review of the literature demonstrating dose-dependent increases in effect at low nanomolar concentrations and cytotoxicity beginning at 1 micromolar concentrations or higher[58,59]. After treatment, cell viability was measured using Trypan blue (Fig. 2A). At 1 µM, 98% and 99% of the cells treated with ADJ-310 and PRL-295, respectively, were alive. Both ADJ-310 and PRL-295 cells maintained a viability of 98% at 5 and 10 µM. The negative control cells treated with DMSO had 98% viability, and the positive control cells treated with CDDO-Me had 100% viability. ADJ-310 and PRL-295 had no significant effect on cell viability compared to that of the control group at any concentration, indicating that

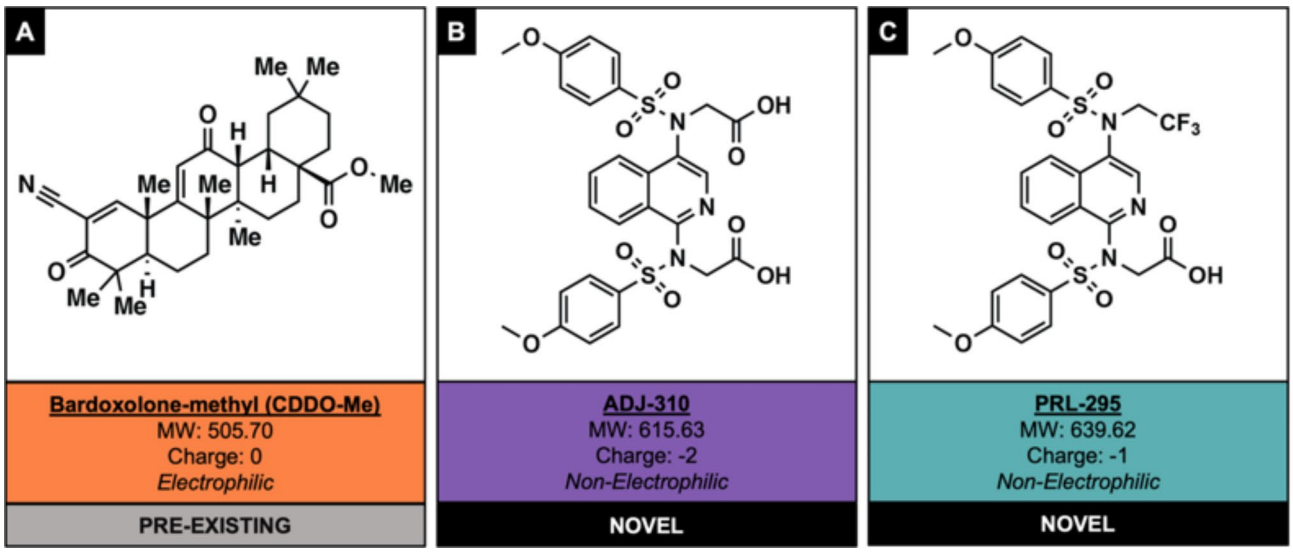

Fig. 1. Chemical structures and properties of ADJ-310, PRL-295, and CDDO-Me. **(A)** The chemical structure of bardoxolone-methyl (CDDO-Me), the preexisting NRF2 activator used as a positive control throughout this work. **(B)** The chemical structures of ADJ-310 and **(C)** PRL-295, the two recently described non-electrophilic NRF2 activators employed in these studies.

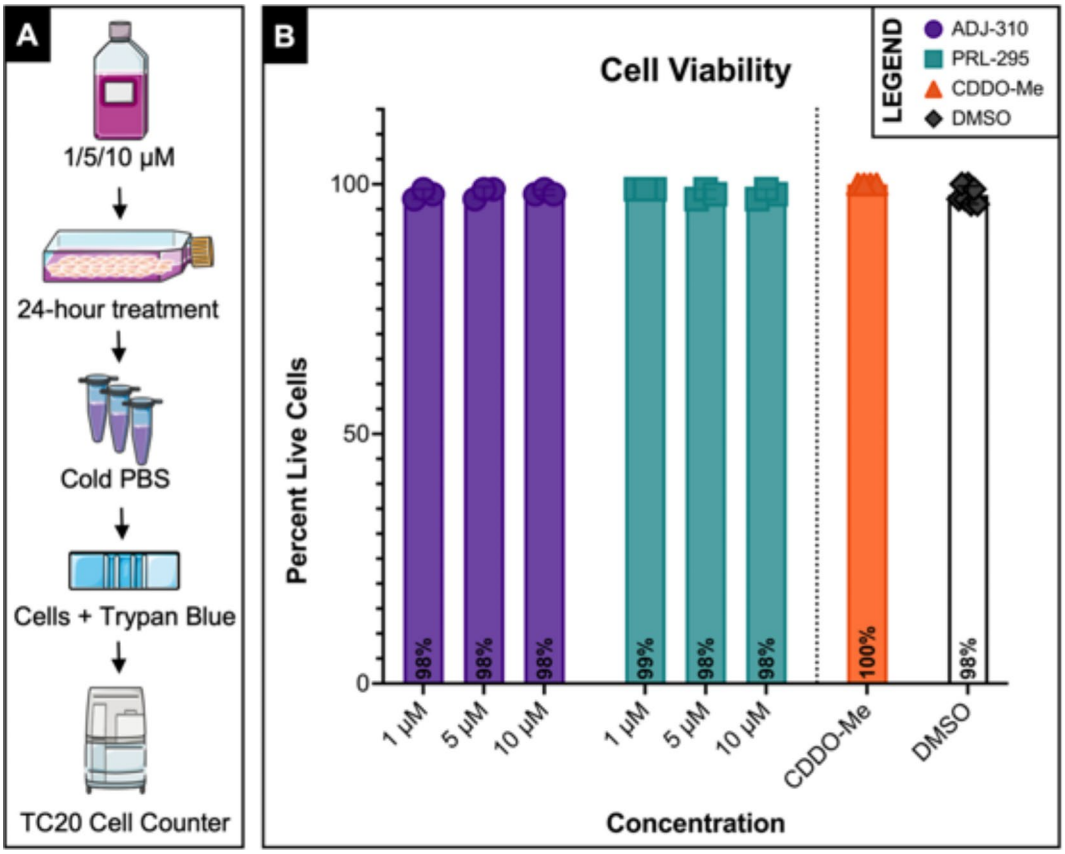

Fig. 2. ADJ-310 and PRL-295 maintain HaCaT cell viability at increasing doses. **(A)** Experimental method: HaCaT cells were treated with 1, 5, or 10 µM of each compound for 24 h, after which viability was measured using Trypan blue. Negative control cells were treated with DMSO only, and positive control cells were treated with 250 nM CDDO-Me. **(B)** A summary of the cell viability assay results is presented as the percentage of live cells. The bars represent the mean values. Individual values are plotted for each group ($n=3$ for all groups except for those treated with CDDO-Me ($n=4$) or DMSO ($n=7$)). Error bars represent the SD. ($N=3$ or greater, * = $P \leq 0.05$, ** = $P \leq 0.01$, *** = $P \leq 0.001$, **** = $P \leq 0.0001$).

the non-electrophilic NRF2 activators maintain cell viability without toxicity, even at increasing concentrations (Fig. 2B).

Next, we examined the effects of these compounds on HaCaT cell proliferation (Fig. 3). Cells were treated with 1, 5, or 10 µM of each compound (ADJ-310 or PRL-295) for 24, 48, or 72 h, after which proliferation was measured using an MTS assay (Fig. 3A), which indirectly measures cell proliferation by quantifying metabolically active mitochondria as a proxy for cell growth and division. Compared with control cells, ADJ-310 and PRL-295 cells exhibited either maintained or increased proliferation at all tested concentrations and time points. At 24 h, compared with the negative control treatment, the 10 µM PRL-295 treatment significantly increased HaCaT cell proliferation ($p<0.05$). At 48 h, compared with the negative ($p<0.0001$) and positive ($p<0.05$) control cells, the PRL-295-treated group exhibited significantly increased HaCaT cell proliferation at both 5 µM and 10 µM, and compared with the negative control cells, the ADJ-310-treated group exhibited significantly increased proliferation ($p<0.0001$) at all three concentrations. At 72 h, compared with the negative ($p<0.01$) and positive ($p<0.05$) control cells, the PRL-295-treated group exhibited significantly increased HaCaT cell proliferation at both 5 µM and 10 µM. These results indicate that ADJ-310 and PRL-295 support normal cell proliferation or enhance proliferation at increasing concentrations and for prolonged periods of time (Fig. 3B).

After characterizing the effects of ADJ-310 and PRL-295 on cell viability and proliferation, we investigated their impact on in vitro wound closure in a cell migration wound model using standardized silicone molds (Fig. 4A). The cells were treated with media containing 10 µM of either ADJ-310 or PRL-295, and cell migration was measured over time. Control cells were treated with either 1% DMSO or 250 nm CDDO-Me. Comparison of wound closure across the four groups demonstrated significant differences in in vitro wound closure over the course of wound healing (2-way ANOVA, $p<0.0001$ overall) and in the overall wound burden, as measured by the calculated area under the curve (AUC) of overall wound closure across replicates (1-way ANOVA, $p<0.0001$ overall) (Fig. 4B-C). Both ADJ-310 and PRL-295 significantly decreased the wound burden ($p<0.0001$) compared to CDDO-Me-treated cells, and PRL-295 also significantly reduced the wound burden ($p<0.05$) compared to DMSO-treated cells. Notably, CDDO-Me significantly impaired wound closure over time and increased the overall wound burden compared to DMSO-treated negative control cells ($p<0.001$) and both ADJ-310 and

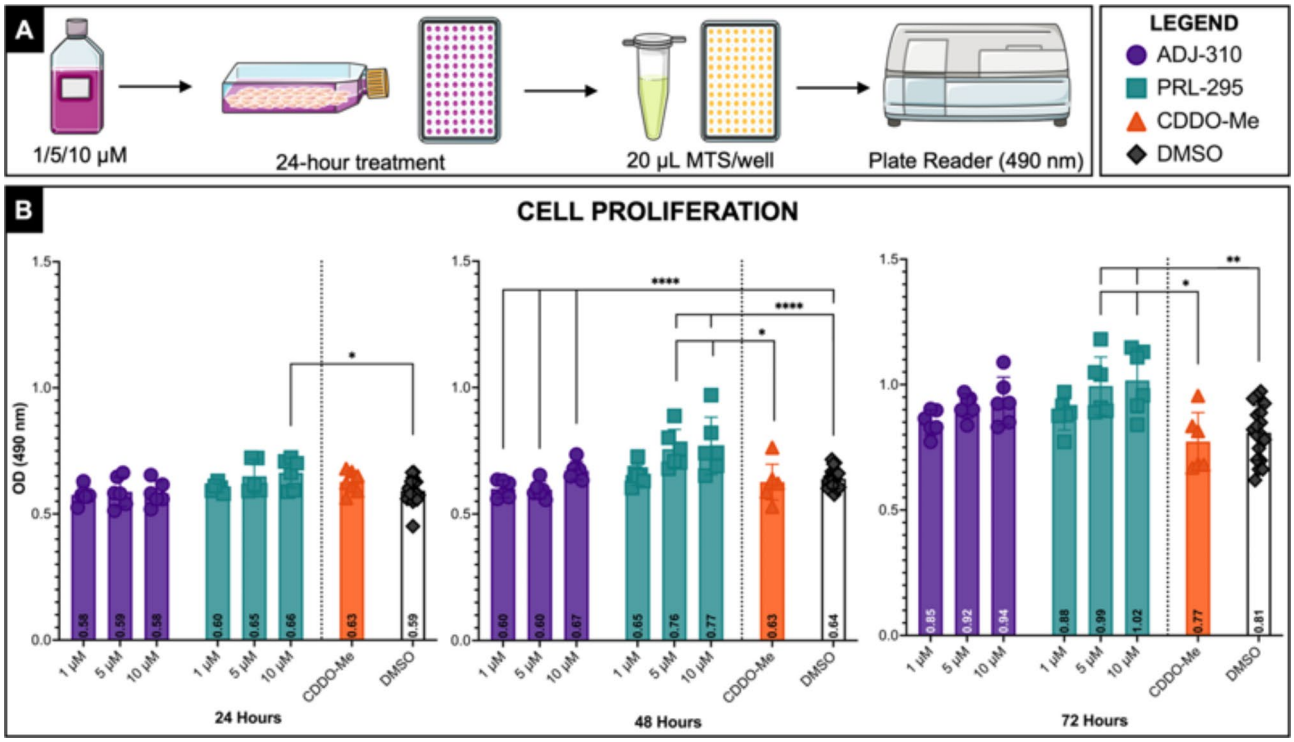

Fig. 3. ADJ-310 and PRL-295 promote HaCaT cell proliferation. **(A)** Experimental method: HaCaT cells were treated with 1, 5, or 10 µM ADJ-310 or PRL-295 for 24, 48, or 72 h, after which proliferation was quantified using an MTS assay. Negative control cells were treated with DMSO only, and positive control cells were treated with 250 nM CDDO-Me. **(B)** A summary of the proliferation results at each time point is presented as the optical density at 490 nm. The bars represent the mean values. Individual values are plotted for each group ($n = 6$ for all groups except for the following: 5 µM PRL-295 at 24 h, for which $n = 5$; CDDO-Me, for which $n = 7$; and DMSO, for which $n = 17$ at 24 and 48 h and $n = 16$ at 72 h). Error bars represent the SD. ($N = 5$ or greater, * = $P \leq 0.05$, ** = $P \leq 0.01$, *** = $P \leq 0.001$, **** = $P \leq 0.0001$).

PRL-295-treated cells ($p > 0.0001$). Both ADJ-310 and PRL-295 significantly increased cell migration compared to that of both control groups. At individual time points, PRL-295-treated cells exhibited significant increases in HaCaT cell migration compared to DMSO-treated control cells at 24 h ($p < 0.0001$), 48 h ($p < 0.0001$), and 72 h ($p < 0.05$) and compared to CDDO-Me-treated control cells at 24 h ($p < 0.0001$), 48 h ($p < 0.0001$), and 72 h ($p < 0.0001$) (Fig. 4D). At individual time points, ADJ-310-treated cells exhibited significant increases in HaCaT cell migration compared to DMSO-treated control cells at 24 h ($p < 0.05$), 48 h ($p < 0.05$), and 72 h ($p < 0.05$) and compared to CDDO-Me-treated control cells at 24 h ($p < 0.0001$), 48 h ($p < 0.0001$), and 72 h ($p < 0.0001$) (Fig. 4D). At all measured time points, CDDO-Me significantly impaired cell migration compared to ADJ-310, PRL-295, and DMSO ($p < 0.0001$ for all comparisons except CDDO-Me vs. DMSO at 24 H, for which $p < 0.05$).

These results indicate that ADJ-310 and PRL-295 improve in vitro wound healing, support keratinocyte survival, promote cell proliferation, and increase cell migration. Notably, PRL-295 had the most promising effects among the two compounds, as it more significantly improved both HaCaT cell proliferation and migration at multiple concentrations and time points.

ADJ-310 and PRL-295 amplify the antioxidant response

We next investigated the effects of ADJ-310 and PRL-295 on the oxidative stress response in HaCaT cells by assessing SOD activity and total glutathione content (Fig. 5A). These assays do not directly measure ROS but rather assess the effects of ADJ-310 and PRL-295 on two major components of the antioxidant response, serving as proof of concept that these compounds appropriately activate responses to oxidative stress. At 10 µM, both ADJ-310 and PRL-295 significantly increased SOD activity compared to that in the control cells (Fig. 5B). Lysates from control cells treated with media containing 10 µL/mL (1%) DMSO exhibited 0.53 U/mL SOD activity, while those from ADJ-310-treated cells exhibited 1.07 U/mL ($q < 0.001$), and those from PRL-295-treated cells exhibited 0.96 U/mL ($q < 0.001$). Lysates from cells treated with 10 µM ADJ-310 or PRL-295 also exhibited significantly greater total GSH levels than did those from control cells (Fig. 5C). Compared with the control cell lysates, the lysates of the ADJ-310-treated cells contained 9.2 µM GSH ($q < 0.0001$), and the PRL-295-treated cell lysates contained 17.1 µM GSH ($q < 0.0001$). At 1 µM, compared with DMSO-treated control cell lysates, which contained 7.4 µM, ADJ-310-treated cell lysates contained 9.5 µM GSH ($q < 0.0001$), and PRL-295-treated cell lysates contained 8.9 µM GSH ($q < 0.001$). Taken together, these results demonstrate that both non-electrophilic NRF2 activators, ADJ-310 and PRL-295, significantly strengthen oxidative stress responses in

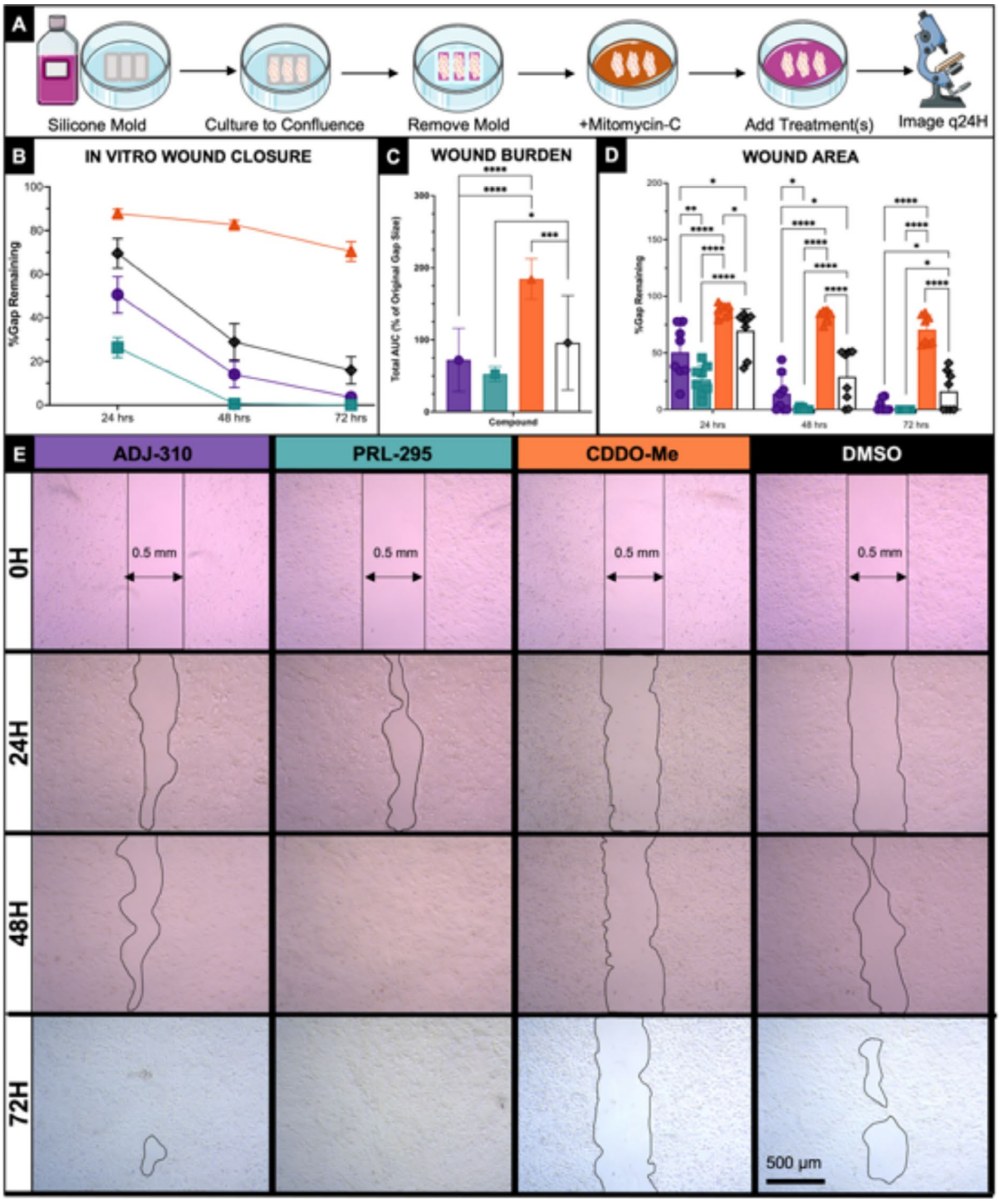

Fig. 4. ADJ-310 and PRL-295 significantly improvein vitro wound closure. **(A)** Experimental method: HaCaT cells were cultured in the wells of a silicone mold until confluent. The molds were removed, and the cells were treated with Mitomycin-C to prevent proliferation. Then, the cells were treated with 10 µM of ADJ-310 or PRL-295, 250 nm CDDO-Me, or 1% DMSO, and the wounds were imaged every 24 h for 3 days. **(B)** A summary of the migration data from 0 to 72 h presented as a percentage of the original wound area. The data points represent the means ($n = 8$), and the error bars represent the SDs. **(C)** Overall wound burden per group, represented as the total normalized area under the curve from the same experiment. The bars represent the mean values ($n = 8$), and the error bars represent the SDs. **(D)** Wound area values from the same experiment at each individual time point are presented as percentages of the original wound size. The bars represent the mean values ($n = 8$), and the error bars represent the SDs. Individual values are plotted for each group. **(E)** Representative photos of in vitro wounds from each group over time. The rows represent 0 H, 24 H, 48 H, and 60 H from top to bottom. The columns represent ADJ-310, PRL-295, CDDO-Me (control) and DMSO (control) from left to right. ($N = 8$, * = $q \leq 0.05$, ** = $q \leq 0.01$, *** = $q \leq 0.001$, **** = $q \leq 0.0001$).

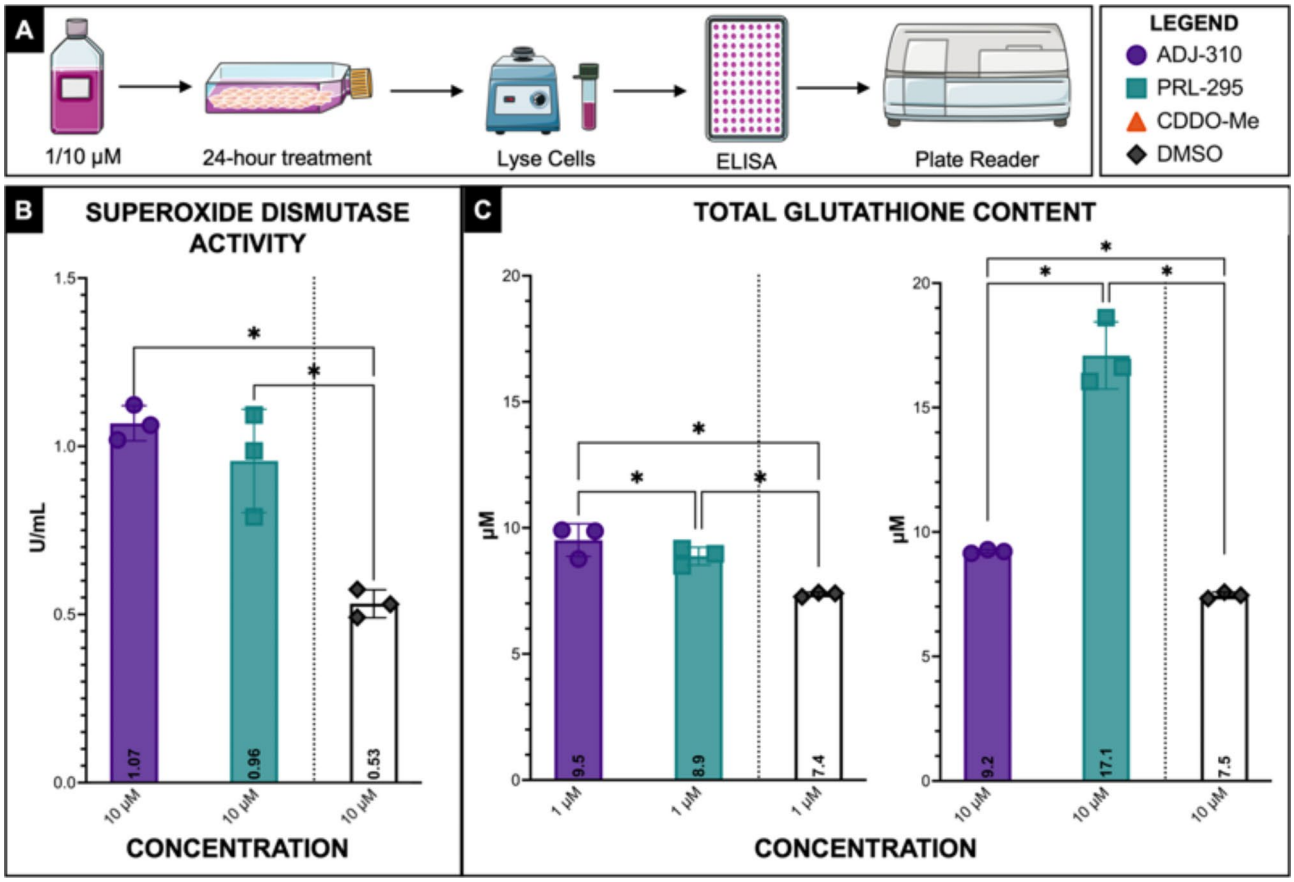

Fig. 5. ADJ-310 and PRL-295 increase oxidative stress responses in HaCaT cells. **(A)** Experimental method: HaCaT cells were treated with 1 or 10 µM of each compound for 24 h. Then, the cells were lysed, and the lysates were analyzed via ELISA. **(B)** The results of the superoxide dismutase (SOD) activity assay presented as SOD activity in U/mL. The bar chart shows the summary of the results at 10 µM. The bars represent the mean values ($n = 3$), and the error bars represent the SDs. Individual data points are plotted for each group. **(C)** Results from the glutathione content assay presented as the total glutathione content in µM. The bar chart shows the summary of the results at 1 and 10 µM. The bars represent the mean values ($n = 3$), and the error bars represent the SDs. Individual data points are for each group. ($N = 3$, * = $q \leq 0.05$, ** = $q \leq 0.01$, *** = $q \leq 0.001$, **** = $q \leq 0.0001$).

human keratinocytes by increasing SOD activity and total GSH content, further demonstrating their efficacy *in vitro*.

mRNA sequencing analysis

To understand the effects of these non-electrophilic NRF2 activators in more detail, we sought to examine the mechanisms driving the response to treatment and to investigate them at the transcriptome level. HaCaT cells were treated with 250 nM CDDO-Me or 10 µM PRL-295 for 14 h ($n = 3$). PRL-295 was selected over ADJ-310 for this analysis both because of the outcomes of the in vitro analyses and because of previous publications supporting its direct mechanism of action and confirming its activation of NRF2[50,56]. The concentration of PRL-295 was selected based on the results of the in vitro experiments, which showed the strongest positive effect on keratinocyte functions at 10 µM. The 250 nM concentration of CDDO-Me was selected based on data demonstrating efficacy without toxicity at sub-micromolar doses[58,59]. After treatment, RNA was extracted, and mRNA sequencing was performed (Illumina NovaSeq, Novogene, USA) (Fig. 6A).

We first assessed the overall number of differentially expressed genes (DEGs) in cells treated with PRL-295 or CDDO-Me (Fig. 6B-D). Within the groups of DEGs, we compared the genes whose expression was most significantly upregulated in the PRL-295- and CDDO-Me-treated cells to that in the control cells. As expected, treatment with either compound significantly increased the expression of many known NRF2 targets, including HMOX1, GCLC, and several AKRs (Fig. 6E). Interestingly, the two groups also had several other upregulated genes in common, such as MAP2, HKDC1, multiple cytochrome P450s, and RP11-227H15.4, although limited literature is available that directly links each of these genes to the NRF2 pathway. A total of 1,373 genes were differentially expressed in PRL-295-treated cells compared to control cells, while 2,422 genes were differentially expressed in CDDO-Me-treated cells —a nearly 1.8X increase in the number of downstream targets. This finding suggests the potential for the engagement of off-targets by CDDO-Me and highlights the narrower

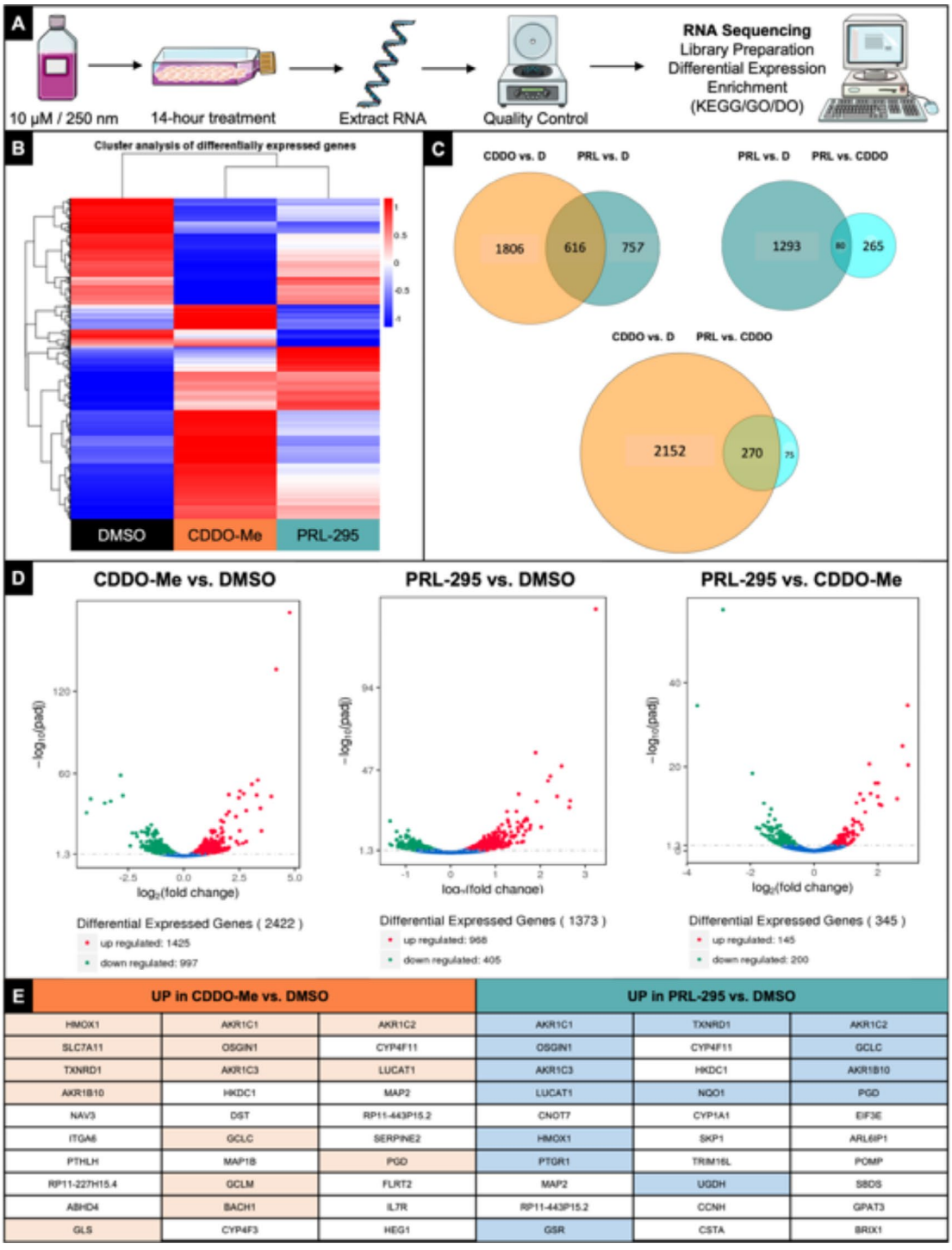

Fig. 6. PRL-295 activates NRF2 with increased specificity and leads to decreased off-target upregulation of disease-related pathways. (A) Experimental method: HaCaT cells were treated with 10 μM PRL-295 or 250 nM CDDO-Me for 14 h ($n = 3$). RNA was subsequently extracted and subjected to mRNA sequencing. **(B)** A heatmap showing the normalized expression of DEGs in control cells, CDDO-Me-treated cells, and PRL-295-treated cells. The results are normalized from the maximum (1, red) to the minimum (-1, blue) based on the log2(FPKM + 1) value. **(C)** Venn diagrams and **(D)** volcano plots comparing the number of DEGs in each group. **(E)** Comparison of the genes whose expression was most upregulated in PRL-295- and CDDO-Me-treated cells, with select well-known NRF2 target genes highlighted. The most significantly upregulated genes in each group are listed in decreasing order from the top left to the bottom right, with rows ranging from left to right. **(F)** Kegg pathways, **(G)** GO terms, **(H)** DO terms, and **(I)** Reactome pathway enrichment bar graphs and dot plots showing the most upregulated pathways in PRL-295- and CDDO-Me treated cells. ($N = 3$, * = $P \leq 0.05$, ** = $P \leq 0.01$, *** = $P \leq 0.001$, **** = $P \leq 0.0001$).

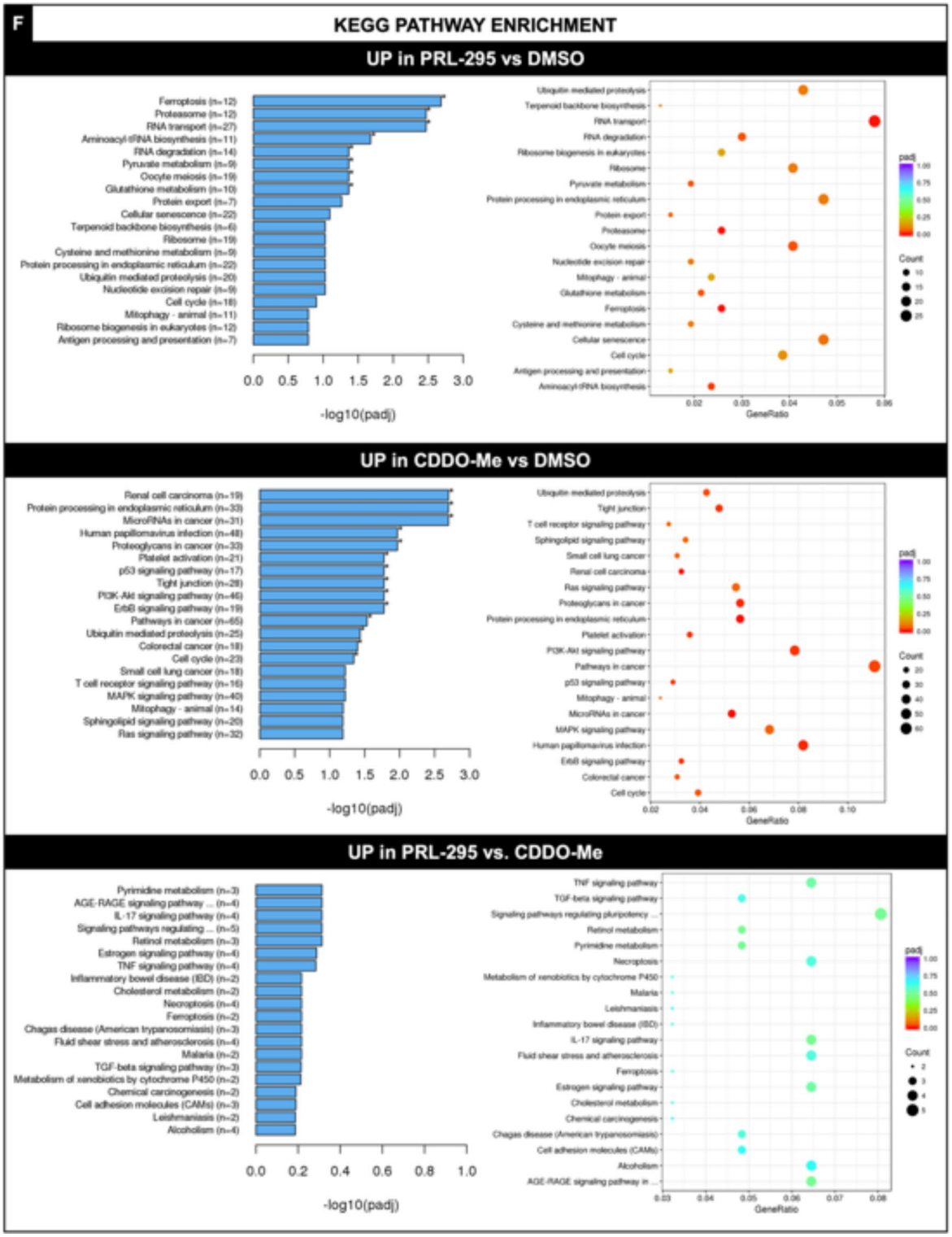

Figure 6. (continued)

transcriptomic effects of PRL-295. Importantly, when considering DEGs compared to those of the controls, the CDDO-Me- and PRL-295-treated cells had 616 DEG targets in common, representing 44.8% of the PRL-295 DEGs but only 25.4% of the CDDO-Me DEGs. These findings suggest that nearly twice as many downstream CDDO-Me target genes may fall outside the NRF2 pathway. When the PRL-295- and CDDO-Me-treated cells were compared, another interesting pattern emerged. A total of 345 genes were differentially expressed between PRL-295-treated cells and CDDO-Me-treated cells. Of those, the majority, accounting for nearly 60% of the DEGs between the two compounds, were downregulated rather than upregulated, suggesting that, compared

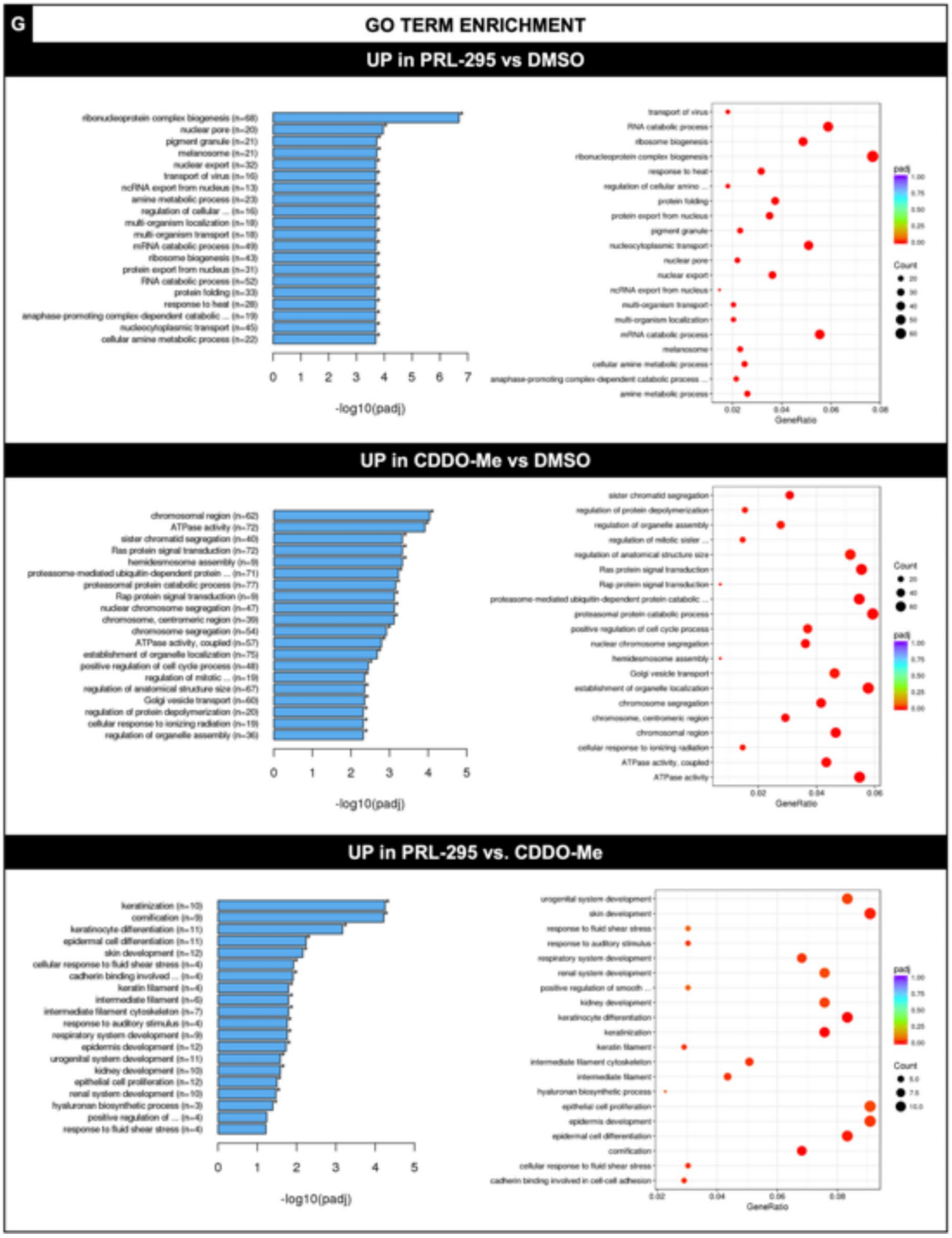

Figure 6. (continued)

with CDDO-Me, PRL-295 targeted genes more specifically and, as a result, showed decreased expression of off-target genes. Similarly, compared to that in the controls, the ratio of upregulated to downregulated genes was 2.4 for the PRL-295-treated cells but only 1.4 for the CDDO-Me-treated cells. As NRF2 is generally considered a positive, rather than negative, regulator, these findings further suggest that the activation profile of PRL-295 is more favorable than that of CDDO-Me.

Next, we investigated the effects of these DEGs on known functional pathways and mechanisms by analyzing the positively enriched Kyoto Encyclopedia of Genes and Genomes (KEGG) (Fig. 6F), Gene Ontology (GO)

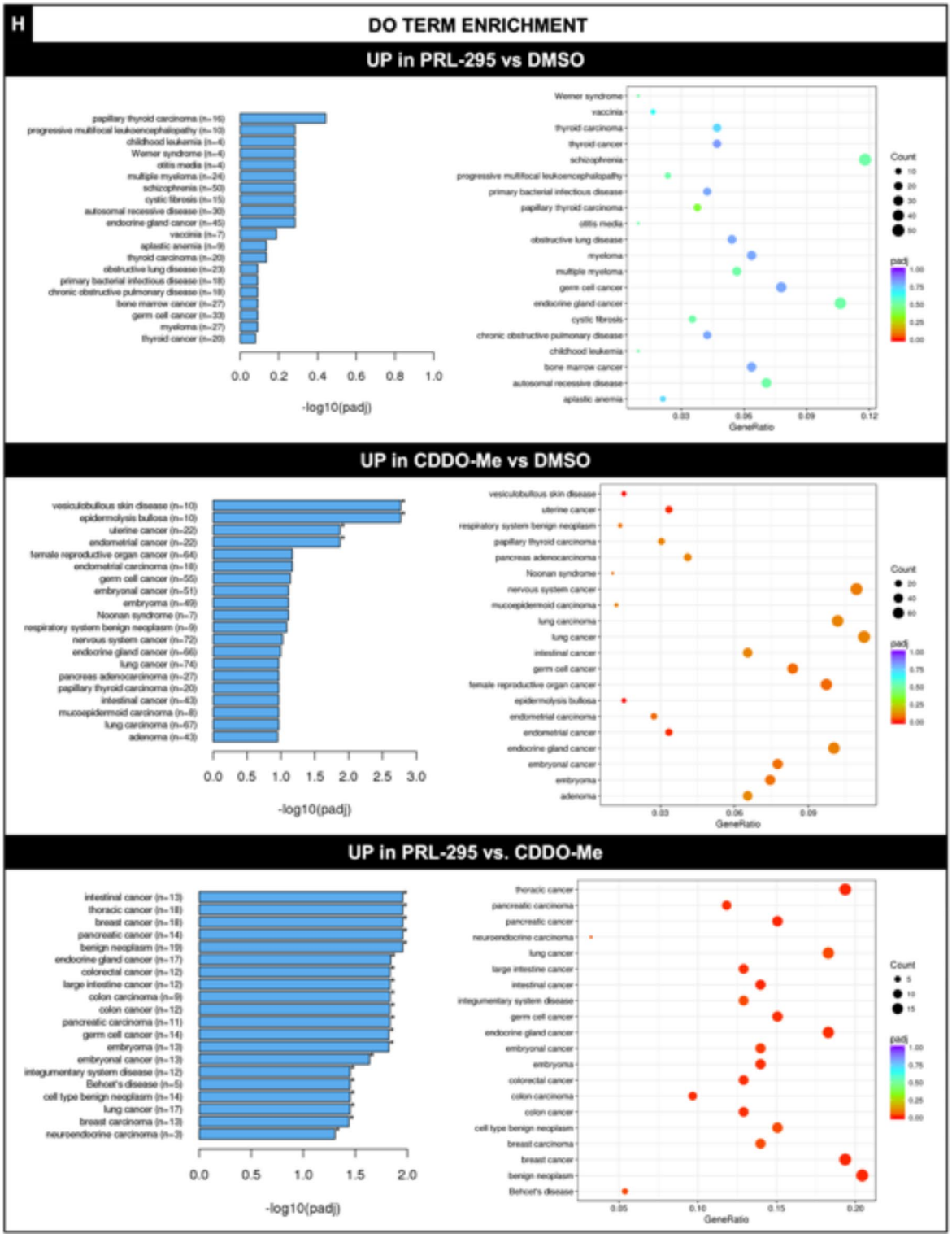

Figure 6. (continued)

(Fig. 6G), Human Disease Ontology (DO) (Fig. 6H), and Reactome (Fig. 6I) pathways in PRL-295- and CDDO-Me-treated cells[60–62]. In the PRL-295-treated cells, there were eight significantly upregulated KEGG pathways compared to those in the controls: ferroptosis, proteasome, RNA transport, aminoacyl-tRNA biosynthesis, RNA degradation, pyruvate metabolism, oocyte meiosis, and glutathione metabolism. In CDDO-Me-treated cells, 14 significantly upregulated KEGG pathways were found, nearly double the number of enriched pathways in PRL-295 cells. These pathways included renal cell carcinoma, protein processing, microRNAs in cancer, human papillomavirus infection, proteoglycans in cancer, platelet activation, the p53 signaling pathway, tight junctions,

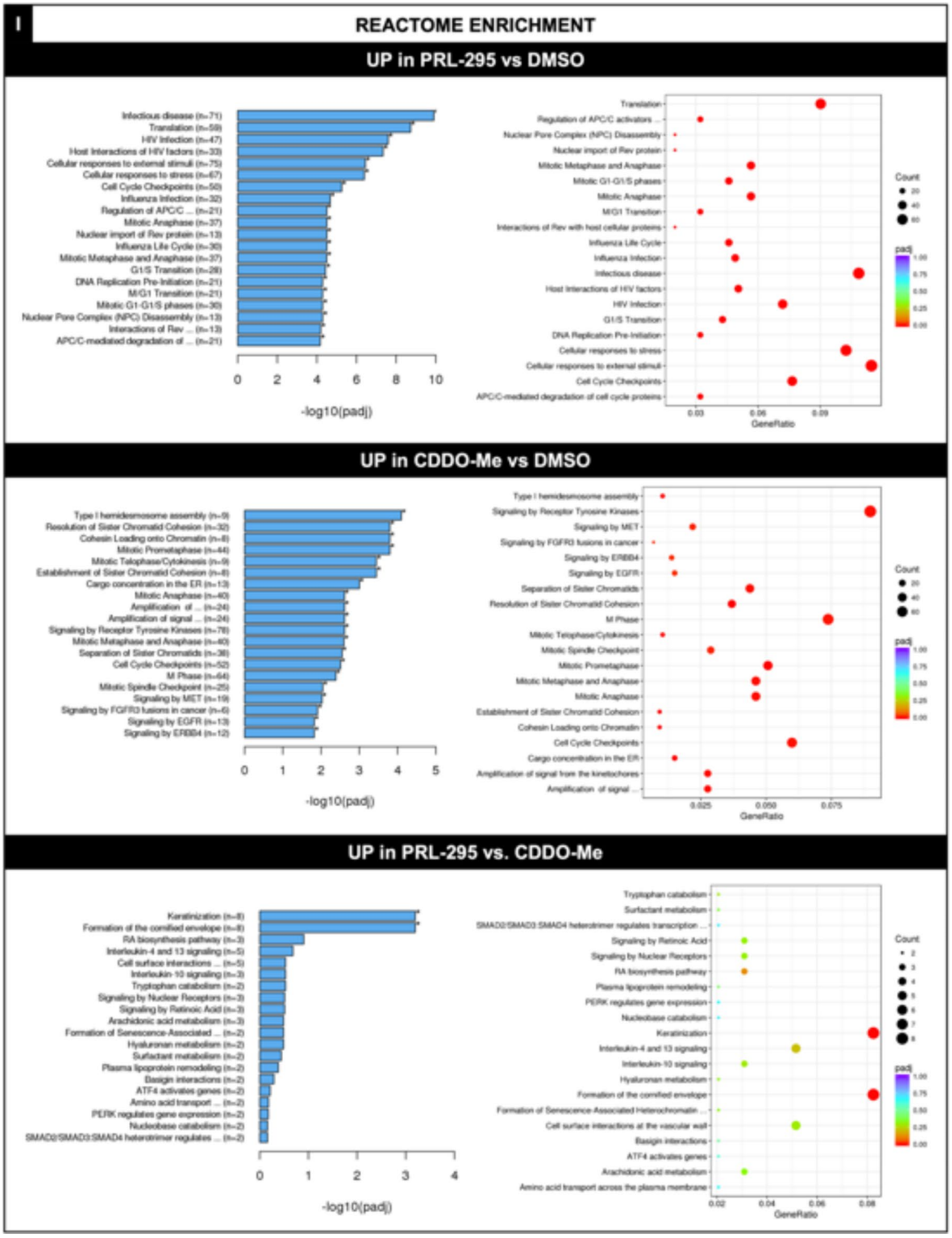

Figure 6. (continued)

PI3K-Akt signaling, ERBb signaling, pathways in cancer, ubiquitin-mediated proteolysis, colorectal cancer, and cell cycle pathways. Interestingly, the two compounds had none of these significantly enriched pathways in common, and only PRL-295 significantly enriched the glutathione metabolism pathway, a key function of NRF2 that did not appear in the top 20 most enriched pathways in CDDO-Me-treated cells. Most importantly, CDDO-Me significantly upregulated multiple disease-associated pathways, with two of its top three most-enriched pathways representing cancer-associated processes. The pathways related to the genes exhibiting significantly upregulated expression also included the p53, AKT, and ERBb signaling pathways, all of which

have been implicated in a variety of cancers, such as breast, colon, ovarian, and lung cancer[30,63–65]. Another key cancer pathway, Ras, is also represented in the top 20 KEGG pathways associated with CDDO-Me. These results demonstrated that, compared with CDDO-Me, PRL-295 improved targeting specificity and, most importantly, demonstrated a widespread reduction in the targeting of known carcinogenic pathways.

Among the significantly upregulated GO terms (Fig. 6G) compared to those of the control-treated cells, many were similar between the PRL-295- and CDDO-Me-treated cells, with the notable exception that Ras signaling was the 4th most significantly enriched term in the CDDO-Me-treated cells but was not present in the top 20 most positively enriched terms in the PRL-295-treated cells. A more interesting pattern was observed when comparing the positively enriched GO terms in the PRL-295- and CDDO-Me-treated cells to one another rather than to those in the control-treated cells. Of the top 18 significantly upregulated GO terms in the PRL-295-treated vs. CDDO-Me-treated cells, nine represented developmental and differentiation pathways for organs and tissues, including the skin, the urogenital system, the kidney and renal system, and the respiratory system. Others include cellular processes that are often involved in healing, including keratinization, cellular response to shear stress, and filament pathways for keratin, intermediate filaments, and the cytoskeleton. These findings suggest that PRL-295 may upregulate pathways relevant to organ function and development and tissue repair to a greater extent than CDDO-Me.

Next, we assessed the DO terms (Fig. 6H) upregulated in response to PRL-295 or CDDO-Me treatment. There were no significantly upregulated DO terms in PRL-295-treated cells compared to control-treated cells, while there were four in CDDO-Me-treated cells: "vesiculobullous skin disease", "epidermal bullosa", "uterine cancer", and "endometrial cancer". When comparing the PRL-295- and CDDO-Me-treated cells, there were more than twenty significantly upregulated DO terms in the PRL-295-treated cells. Interpretation of these findings is challenging, as PRL-295-treated cells demonstrated no significant differences in DO term expression compared to control-treated cells, indicating that although there were significant differences between the two compounds, these differences represent only relative differences, and PRL-295 exhibited no significant effect on any DO term independently. Additionally, the four DO terms significantly enriched in the CDDO-Me-treated cells compared to the control cells were not present among the 20 most enriched terms between PRL-295 and CDDO-Me.

Finally, compared with control cells, both PRL-295- and CDDO-Me-treated cells exhibited 20 + upregulated Reactome pathways (Fig. 6I), which was expected given the many roles of NRF2 in cellular processes and metabolism. Many of the upregulated pathways, including several related to mitosis, the cell cycle, DNA replication, and cellular signaling, were similar among cells treated with each compound. In this case, both compounds upregulated a small number of Reactome pathways involved in human disease, including cancer signaling and infection pathways. Only two Reactome pathways were significantly upregulated in PRL-295-treated cells compared to those treated with CDDO-Me: keratinization and the formation of the cornified envelope. These results reflect both the shared function of these compounds in activating NRF2 and the breadth of the functions of NRF2 in essential cellular processes.

According to the RNA-seq analysis, PRL-295 exhibited narrower downstream target activation, reduced upregulation of multiple disease-associated pathways, and an overall reduction in gene activation. These findings suggest that PRL-295 and its family of non-electrophilic compounds may be more selective NRF2 activators than their electrophilic counterparts.

ADJ-310 and PRL-295 improve diabetic wound healing and activate downstream NRF2 target genes in vivo

Having confirmed the efficacy of ADJ-310 and PRL-295 in promoting in vitro wound healing and examined the downstream pathways of PRL-295 compared to those of CDDO-Me, we next investigated their effects on diabetic wound healing in vivo using *Lepr*$^{db/db}$ mice, a well-studied model of type 2 DM (Fig. 7). Eight-week-old female mice were each given two full-thickness dorsal skin wounds, which were imaged and treated topically with 100 µg of ADJ-310, PRL-295, or CDDO-Me per wound each day. In the first experiment ($n = 11$), ADJ-310 was administered in a solution of 40% DMSO in PBS, the lowest concentration of DMSO that fully dissolved the compound (Fig. 7B-E). In the second experiment ($n = 6$), both ADJ-310 and PRL-295 were administered in 25% F-127 Pluronic Gel and 10% DMSO in PBS (Fig. 7F-I).

In the first study, ADJ-310 significantly improved wound closure over the course of healing (2-way ANOVA, $p = 0.0057$), with the largest difference in wound size observed in the first 8 days of healing (Fig. 7B). The wound burden was also 15.2% lower in the ADJ-310-treated group than in the control group (Fig. 7C). Although the difference was not statistically significant, this finding indicates biological relevance, as a change in the wound area is a critical factor in wound closure outcomes in human patients, for whom the percent change in the wound area in the first third of healing time is a significant predictor of wound closure[66]. Additionally, the high concentration of DMSO in the vehicle solution may be a potential complication due to the diverse findings regarding its positive and negative effects on wound healing. To address this issue and reduce variability, the second study was conducted using a Pluronic gel vehicle containing only 10% DMSO.

In this iteration, we focused specifically on the first eight days of healing, as suggested by the results of the previous study, and investigated the effects of ADJ-310, PRL-295, and CDDO-Me on wound healing. As expected, all three compounds significantly improved wound closure over time compared to that of the controls (2-way ANOVA, $p = 0.04$) (Fig. 7F). In addition, the wound burden was significantly lower in all three treatment groups (one-way ANOVA, $p = 0.0089$), with ADJ-310 reducing the burden by 14.3% ($q < 0.05$), PRL-295 reducing the burden by 11.7% ($q < 0.05$), and CDDO-Me reducing the burden by 17.2% ($q < 0.01$) (Fig. 7G). Furthermore, the treated wounds were significantly smaller at the individual time points on D6 ($p = 0.0042$), D7 ($p = 0.0372$), and D8 ($p = 0.0190$) for ADJ-310 and on D3 ($p = 0.0422$) and on D7 for PRL-295 ($p = 0.0225$) (Fig. 7H).

Finally, we repeated this in vivo experiment and harvested the treated wounds on D1, six hours after treatment with either ADJ-310, PRL-295, or a solution of 25% F-127 Pluronic gel (PG) and 10% DMSO in PBS

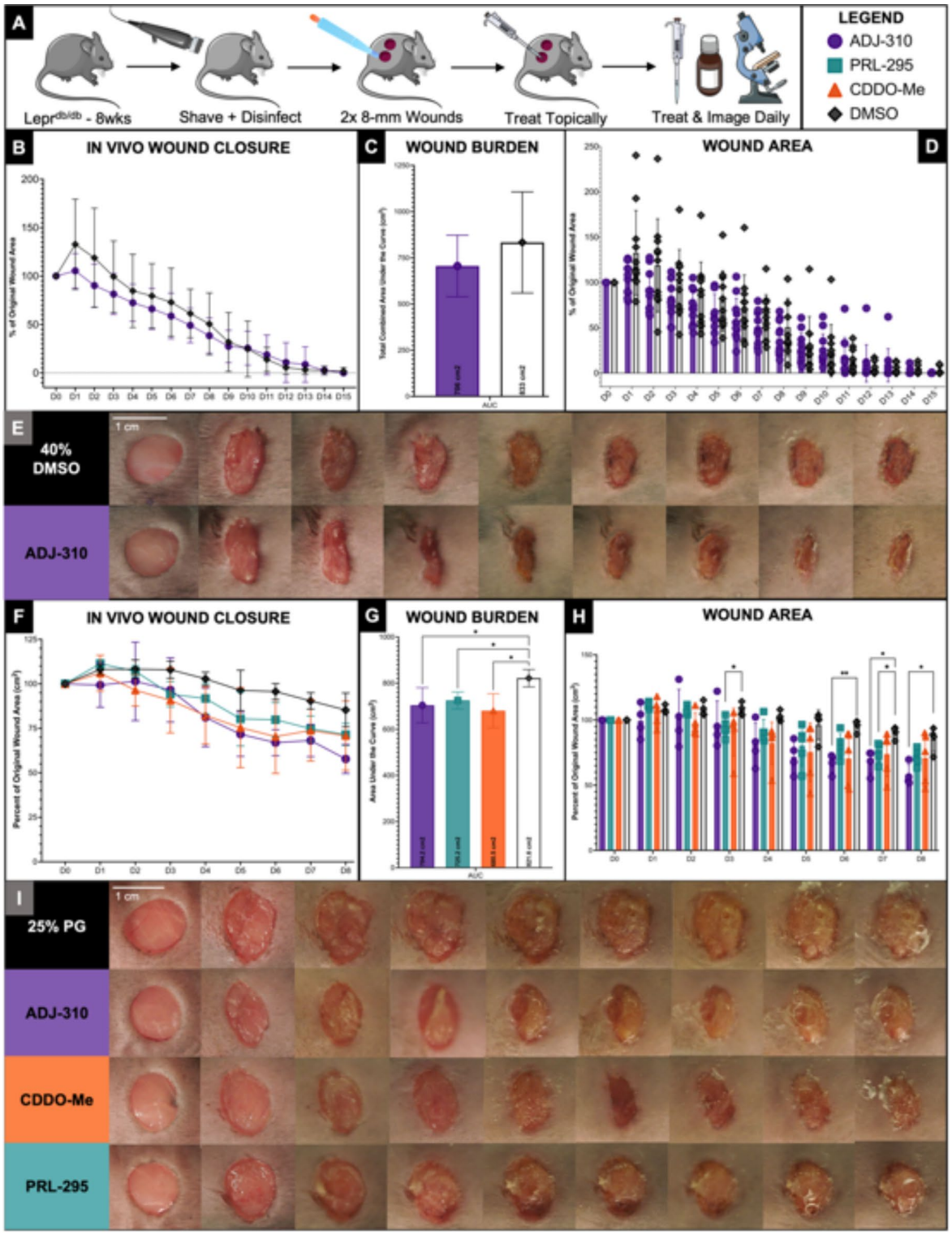

as above. RT-PCR analysis of the harvested tissue showed that treatment with ADJ-310 or PRL-295 activated known downstream NRF2 target genes in vivo (Fig. 8A). Four well-known and well-studied downstream target genes were selected for evaluation: Gclc, Gclm, Nqo1, and Mox1. All primers used were mouse species and are listed in Fig. 8D. Compared to DMSO alone, ADJ-310 significantly upregulated Gclc expression in treated wounds ($p < 0.05$), and PRL-295 significantly upregulated both Gclc ($p < 0.001$) and Gclm ($p < 0.05$) expression in treated wounds (Fig. 8B). ADJ-310 also increased expression of Gclm ($p = 0.067$). When compared together, ADJ-310 and PRL-295 significantly upregulated expression of these genes in vivo compared to control-treated wounds ($p > 0.001$ by 2way ANOVA overall) (Fig. 8C). In the combined comparison, both ADJ-310 and PRL-295 significantly upregulated expression of Gclc ($q < 0.05$ for ADJ-310, $q < 0.01$ for PRL-295) and Mox1 ($q < 0.05$ for ADJ-310, $q < 0.001$ for PRL-295) (Fig. 8C).

◀**Fig. 7**. ADJ-310 and PRL-295 significantly improve diabetic wound healingin vivo. **(A)** Experimental method: Eight-week-old female *Lepr*$^{db/db}$ mice were each given two 8-mm diameter full-thickness dorsal skin wounds, which were imaged and treated topically each day with 100 µg of each compound. Panels **B-E** and **F-I** show the results of two different experiments. **(B)** A summary of the wound closure results from an experiment testing ADJ-310 in a vehicle solution of 40% DMSO in PBS ($n = 11$). **(C)** Overall wound burden per group, represented as the total normalized area under the curve from the same experiment (ADJ-310 vs. DMSO). **(D)** Wound area values from the same experiment at each individual time point presented as percentages of the original wound size. **(E)** Representative photos of in vivo wounds from each group over time. The rows represent the control- (40% DMSO in PBS) and ADJ-310-treated wounds. The columns represent D0–D8 from left to right. **(F)** A summary of the wound closure results from an experiment testing ADJ-310, PRL-295, and CDDO-Me in a vehicle solution of 25% F-127 Pluronic Gel (PG) and 10% DMSO in PBS ($n = 4$ for ADJ-310 and PG, $n = 5$ for PRL-295 and CDDO-Me). **(G)** Overall wound burden per group and **(H)** wound area values from the same experiment at each individual time point presented as percentages of the original wound size. **(I)** Representative photos of in vivo wounds from each group over time. The rows represent the controls (PG), ADJ-310, CDDO-Me, and PRL-295 from top to bottom. The columns represent D0–D8 from left to right. The bars and data points in all panels represent the means, and the error bars represent the SDs. Individual data points are plotted for each group in panels D and H. ($N = 11$ for A-E; $N = 4$ for ADJ-310 and PG, $N = 5$ for PRL-295 and CDDO-Me for F-I; * = $P \leq 0.05$, ** = $P \leq 0.01$, *** = $P \leq 0.001$, **** = $P \leq 0.0001$).

Taken together, these results indicate that non-electrophilic NRF2 activators ADJ-310 and PRL-295 improve diabetic wound healing in vivo and, notably, do so comparably to CDDO-Me, a well-studied, clinically used NRF2 activator. They also confirm the upregulation of known downstream NRF2 targets in treated tissues. These findings confirm the efficacy and usability of ADJ-310 and PRL-295 for studying the role of NRF2 in disease processes in vivo.

Discussion

In the nearly 30 years since the discovery of NRF2, thousands of publications have sought to elucidate its functions, discuss its roles, and unlock its potential. Along the way, naturally occurring NRF2 activators such as sulforaphane, which is isolated from broccoli, and curcumin, which is isolated from turmeric plants, as well as synthetic compounds such as bardoxolone and omaveloxolone, have been employed to understand the pathway and harness it for clinical use. More than 30 clinical trials have studied the effects of bardoxolone on a variety of cancers, Alport syndrome, pulmonary hypertension, various kidney disorders, interstitial lung disease, and even COVID-19 (via *ClinicalTrials.Gov*); however, these trials have yielded limited success. Since the FDA approval of Tecfidera (dimethyl fumarate) in 2013, few additional NRF2-activating therapies were approved until a similar drug, Vumenity (diroximel fumarate) was approved in 2019, followed by Skyclarys (omaveloxone), which became the first and only FDA-approved medication for the treatment of Friedrich's Ataxia in March 2023. As the understanding of NRF2 functions has increased, so too has the need for improved NRF2 activators[31].

In this work, we investigated two recently described non-electrophilic NRF2 activators, ADJ-310 and PRL-295. We first demonstrated that human keratinocytes survive in culture at increasing doses of both ADJ-310 and PRL-295 (Fig. 2). Next, we showed that ADJ-310 and PRL-295 support or improve cellular proliferation (Fig. 3) and improve in vitro wound closure (Fig. 4). We also showed that both ADJ-310 and PRL-295 enhanced oxidative stress responses in keratinocytes by increasing SOD activity and total glutathione content (Fig. 5). These assays served as important validation experiments confirming the in vitro efficacy and usability of ADJ-310 and PRL-295; however, they are not without limitations. The MTS assay used in the proliferation study quantifies mitochondrial metabolic activity as a proxy for cell proliferation, but it does not exclusively reflect changes in cell number, and, given the known role of NRF2 in modulating cellular metabolism, it is possible that a component of the observed increases reflects increased cellular metabolic activity due to NRF2 in addition to increased cell number alone. The SOD and glutathione assays offer evidence that both ADJ-310 and PRL-295 activate the oxidative stress response as expected, and future work, such as direct measurement of ROS and ARE reporter gene assays, will allow us to better confirm and categorize the oxidative response after treatment with these compounds.

Importantly, neither of the compounds showed cytotoxicity or suppression of the assessed cell functions at increasing doses, suggesting that they may offer broader therapeutic windows, an important consideration for potential use in future clinical studies or as therapeutics. This feature is particularly relevant in comparison to electrophilic NRF2 activators such as CDDO-Me and its counterparts, which upregulate NRF2 target genes at concentrations as low as 1 to 10 nM but quickly begin to demonstrate significant cytotoxicity at concentrations as low as 1 µM and above[58,59]. This narrow therapeutic window poses many challenges for clinical translation, but the duality of these compounds is not without its limitations: several clinical investigations of CDDO-Me rely directly on these proapoptotic effects at relatively high doses for anticancer effects, making the drug ambidextrous in many ways[67]. This narrow range of concentrations also posed a critical question during the design of these experiments to ensure that the concentration was high enough to produce comparable effects but not so high that cytotoxicity skewed the results. According to the literature on CDDO-Me and related compounds, doses in the µM range or higher regularly induce apoptosis, while doses throughout the nM range demonstrate predominantly antioxidant and cytoprotective effects, often with dose-dependent increases in NRF2 target gene expression, antioxidant enzyme activity, glutathione content, etc[58,59]. Consequently, we selected 250 nM CDDO-Me as our positive control because of the dose-dependent increase in effects while remaining well below the threshold for toxicity. Throughout the in vitro experiments presented here, no differences were

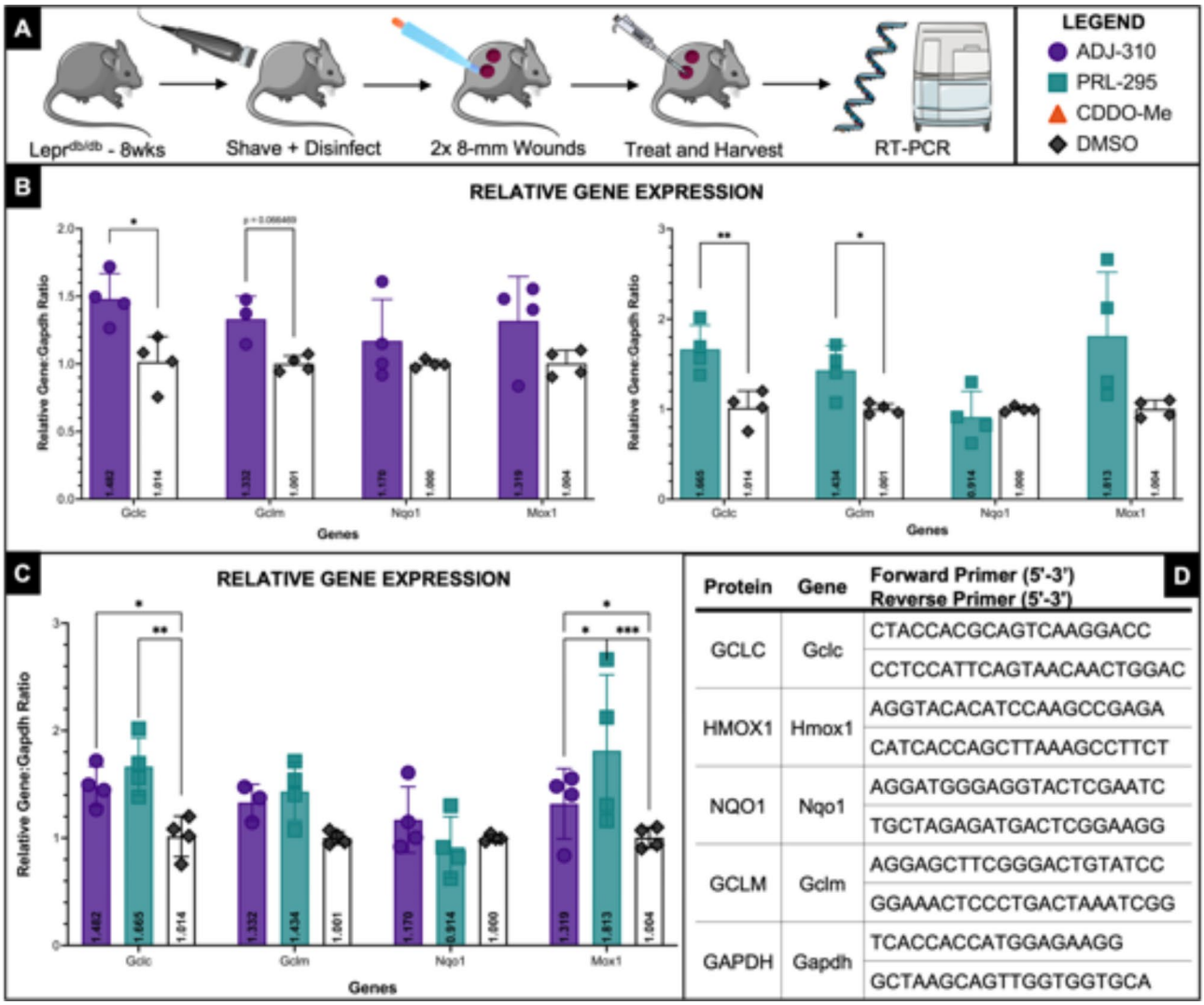

Fig. 8. ADJ-310 and PRL-295 upregulate NRF2 target genesin vivo. **(A)** Experimental method: Eight-week-old female *Lepr*$^{db/db}$ mice were each given two 8-mm diameter full-thickness dorsal skin wounds, which were imaged and treated topically with 100 µg of each compound immediately after wounding on D0 and again on D1. Wounds were harvested 6 h after treatment on D1, and RNA was extracted for RT-PCR. **(B)** Relative gene expression of NRF2 target genes compared to GAPDH in compound-treated vs. DMSO-treated wounds. Data shown represent isolated comparison of either ADJ-310 or PRL-295 to DMSO by multiple two-tailed unpaired t-tests with Welch's correction. **(C)** Relative gene expression of NRF2 target genes compared to GAPDH in compound-treated vs. DMSO-treated wounds. Data shown represent comparison of ADJ-310, PRL-295, and DMSO by two-way ANOVA. **(D)** Primer sequences used for RT-PCR. The species was mouse for all primers used. The bars in all panels represent the mean values ($n = 4$), and the error bars represent the SDs. Individual values are plotted for each group. ($N = 4$ biological replicates, each consisting of 2 technical replicates, * = $P \leq 0.05$, ** = $P \leq 0.01$, *** = $P \leq 0.001$, **** = $P \leq 0.0001$).

observed between the positive and negative control groups except for in the cell migration study, which further confirmed the selection of this midrange concentration for CDDO-Me. Interestingly, both the cell proliferation and cell migration assay included 250 nM CDDO-Me for comparison, and both assays ran over 72 h, yet only the migration assay demonstrated impairment in the response of CDDO-Me-treated cells, suggesting that this finding may not be concentration dependent but, rather, may represent expected variability in the effects of CDDO-Me on different cellular functions.

In considering the appropriate concentrations for this work, we also faced the challenges of solubility and drug delivery method. We have previously shown that these non-electrophilic activators have good stability in liver microsomes, easing concerns about degradation during the time course of our experiments[68]. Likewise, the $LogD_{7.4}$ values of these compounds are low, implying good partitioning into aqueous environments[68]. We prioritized topical application throughout this work both to limit systemic effects of the compounds and DMSO and to address practical considerations regarding topical vs. systemic therapies in clinical use. For many DFU patients, topical therapies offer a simpler and more accessible treatment option, so we emphasized this form of

administration in our investigation. In these studies, we used simple formulations to minimize confounding effects. We will explore more complex, clinically appropriate drug-delivery systems in the future.

A critical challenge surrounding many previously studied NRF2 activators is their lack of selectivity, which leads to off-target effects[51–53]. Many of these compounds are also known to target proteins involved in cancer and other diseases, and multiple clinical trials employing NRF2 activators have failed due to a range of issues, including cytotoxicity[41,42]. As a result, progress toward targeting NRF2 as a potential therapeutic has been hampered, underscoring the need for improved NRF2 activators that can unlock the potential of this transcription factor while limiting associated risk[28,39]. To address the specificity and underlying mechanism, we performed an mRNA sequencing study comparing PRL-295-treated cells and CDDO-Me-treated cells (Fig. 6). This study revealed that CDDO-Me differentially regulated nearly twice as many genes as PRL-295 did and positively enriched more cancer- and disease-associated KEGG and GO pathways, suggesting that PRL-295 may activate NRF2 with greater specificity and narrower, more selective transcriptomic effects. These results are promising indications that non-electrophilic activation of NRF2 may result in decreased off-target binding.

However, there are important caveats to consider in the interpretation of these findings. Specifically, NRF2 has been shown to have both carcinogenic and anticancer effects, which depend largely on the type and stage of the cancer and the magnitude of NRF2 activation. This paradox led to the "double-edged sword" nickname of the NRF2 pathway with respect to cancer; some cancers propagate by constitutively activating NRF2, while in others, NRF2 activation protects normal tissue against cancer-induced oxidative stress and inflammation[69]. Additionally, known cancer pathways in the KEGG and GO terms include both proto-oncogenes and tumor suppressor genes, as well as the intermediate genes responsible for both the development of and response to various cancers. When a given disease-related KEGG or GO term is differentially expressed, it is difficult to ascertain whether the net outcome promotes or inhibits the disease of interest without further investigation into the relative expression levels and functions of the pathway genes collectively. Furthermore, it is expected that any two different compounds would result in different expression patterns, even if those two compounds are from a similar class or share a mechanism of action. It is difficult to determine the extent to which variability in expression patterns between PRL-295 and CDDO-Me is specifically due to reduction in off-target binding rather than to other effects (e.g., some degree of expected variability, differences in drug potency, potential effects on the other functions of Keap1 beyond its role in binding NRF2). The transcriptomic expression patterns of PRL-295-treated cells compared to those of CDDO-Me-treated cells offer initial insights into the specificity and downstream targeting of these non-electrophilic NRF2 activators. Future work will allow us to compare gene expression patterns across other NRF2-activated conditions, such as Keap1-overexpressing cells, and in NRF2 knockout models. Recent transcriptomic studies by Hamblet et al. comparing KEAP-1 inhibitors to direct NRF2 overexpression by modified RNAs have already begun to evaluate these variable expression patterns in vitro in human lung cells[70]. The narrower transcriptomic effect of PRL-295 compared to CDDO-Me observed in the present work offers a potential benefit in investigating the effects of NRF2 with more refinement. Especially when considering NRF2's widespread roles in disease processes and its prominent investigation as a potential therapeutic, activating the downstream targets more narrowly offers the opportunity to limit undesired effects and potentially identify more specifically its different roles in each disease state. This reduction in overall gene activation could also offer a translational benefit in future drug development, potentially reducing possible side effects and complications by reducing the number of unintentionally affected genes.

Finally, we assessed the efficacy of these compounds in vivo and found that both ADJ-310 and PRL-295 significantly improved wound healing in diabetic mice (Fig. 7) and upregulated known NRF2 target genes in treated wounds (Fig. 8). The in vivo improvements in wound healing were in line with those observed in CDDO-Me-treated mice, highlighting that these non-electrophilic compounds have efficacy comparable to that of preexisting compounds in improving diabetic wound closure in the *Lepr*$^{db/db}$ model. Although this demonstration of noninferiority in improving wound healing supports the implementation of this family of non-electrophilic NRF2 activators in future investigations, there remains a critical question regarding the clinical significance of the observed findings in diabetic mice and, subsequently, whether NRF2 activators may be better employed in other clinical and research questions. Although the results demonstrated here highlight the efficacy of ADJ-310 and PRL-295, the translatability of these results in diabetic mice to human subjects is not guaranteed due to several complicating factors, including the closure of mouse wounds by muscular contraction, the complexity of the human DFU, and the multifactorial nature not only of diabetes itself but also of the wound environment. As the DFU has posed an increasingly evasive clinical challenge, hundreds of factors have been investigated in search of an effective treatment; however, even those with the strongest preclinical evidence in rodent models have shown minimal efficacy in clinical trials, and among the very few that have reached widespread clinical use, efficacy among the general diabetic population remains limited[2]. This large body of work frames a significant challenge: the human diabetic wound—and the patient who develops it—is so complex and multifactorial that single-factor or even single-pathway treatments may not be sufficient for treating DFUs in the real patient population. As such, our studies provide proof of concept that a multicomponent treatment regimen that includes pharmacological NRF2 activators may be useful in the development of therapeutics for treating DFUs.

Taken together, these findings establish the non-electrophilic small-molecule NRF2 activators ADJ-310 and PRL-295 as innovative tools for the study of the NRF2 pathway and its functions. These compounds are effective both in vitro and in vivo, demonstrate comparable in vivo efficacy to preexisting compounds, and show narrower downstream gene activation, making them favorable options that directly address the concern of off-target effects among electrophilic NRF2 activators and offer the potential for more refined investigation of downstream targets. While this work began with one specific disease target – the chronic diabetic wound – these findings are broadly applicable and serve to expand the opportunities for the study of NRF2 and its role in multiple disease states.

Materials and methods

HaCaT cell culture

Spontaneously immortalized human keratinocytes (HaCaT cells) were purchased from AddexBio (San Diego, CA, USA, Catalog #T0020001) in 2017 and maintained in frozen aliquots. For cell migration assays, HaCaT cells were propagated in Dulbecco's modified Eagle's medium (DMEM) (4.5 g/l glucose, sodium pyruvate, L-glutamine) (Mediatech, Manassas, VA, USA) supplemented with 10% FBS (GeminiBio, Sacramento, CA, USA) and penicillin-streptomycin (0.1%) (Life Technologies, Carlsbad, CA, USA) or in DermaLife K Keratinocyte Complete Medium (Lifeline Cell Technology, Frederick, MD, USA, Catalog # LL-0007) containing D-Glucose (6 mM), insulin (5 µg/mL), L-Glutamine (6 mM), epinephrine (1 µM), apo-transferrin (5 µg/mL), TGF-α (0.5 ng/mL), pituitary extract (0.4%), and hydrocortisone hemisuccinate (100 ng/mL). For all other in vitro experiments, HaCaT cells were cultured in Dulbecco's modified Eagle medium (DMEM) supplemented with L-glutamine, sodium pyruvate, and phenol red without HEPES (*N*-2-hydroxyethylpiperazine-*N*'-2-ethanesulfonic acid) buffer. The media contained 1 g/dL glucose, corresponding to normal blood glucose levels in mice (Jackson Labs, Strain #000642). All cells were grown in adherent cell and tissue culture plates or flasks (Falcon/Corning, Thermo Fisher Scientific, Waltham, MA).

All cells were incubated at 37 °C and 5% CO_2 in a ThermoForma Series II Water Jacketed incubator (Thermo Fisher Scientific) and used once they reached 80–90% confluence. For cell line maintenance, splitting, or use in experiments, cells were detached from plates using TrypLE reagent (Thermo Fisher Scientific). All cell culture procedures were performed in a SterilGARD III Advance culture hood (The Baker Company, Sanford, ME) using a sterile technique.

Preparation of treatment solutions

For all the experiments, treatment solutions were freshly prepared each day to ensure consistency and prevent degradation. ADJ-310 and PRL-295 were synthesized as previously described[54,55,68,71,72], with purities of 98% or greater. CDDO-Me was obtained from AdooQ Bioscience (CAS NO. 218600-53-4, Irvine, CA). For in vitro assays, a 1 mM stock solution was prepared by mixing the appropriate mass of solid powder compound with 100% dimethylsulfoxide (DMSO). This stock solution was then diluted in DMEM to make working solutions with concentrations of 0.25, 1, 5, or 10 µM for each compound. Where appropriate, additional DMSO was added to the working solutions to ensure that all the solutions contained an equal volume of DMSO (10 µL/mL, or 1%). For in vivo assays, solutions were prepared by first dissolving the appropriate amount of solid powder compound in 100% DMSO. The stock solution was then diluted to a final concentration of 40% DMSO in PBS, and 100 µg of compound was added to 30 µL of solution. All the solutions were prepared using sterile reagents.

Cell viability

HaCaT cells were cultured as described above until confluent. The cells were then treated for 24 h (h) with media containing 1, 5, or 10 µM of each compound (ADJ-310 or PRL-295). Negative control cells were treated with 10 µL/mL DMSO (1% final concentration) in media. Positive control cells were treated with media containing 250 nM CDDO-Me. After treatment, the cells were detached as above and then centrifuged for 5 min at 1,400 rpm. The TrypLE reagent was removed, and the cell pellets were washed and resuspended in cold PBS. Cell viability was subsequently measured using a TC20™ Cell Counter (Bio-Rad, Hercules, CA) with a 1:1 ratio of Trypan blue (Thermo Fisher Scientific) and a HaCaT cell suspension. Briefly, 10 µL of a 50/50 mixture of cell suspension and Trypan blue was pipetted into a well on specialized TC20™ Cell Counter slides. The slide was subsequently inserted into a TC20™ Cell Counter machine, which detects the presence of Trypan blue and provides a cell viability reading (percent live cells).

Cell proliferation

Cell proliferation was measured using the CellTiter 96 AQueous One Solution Cell Proliferation Kit, referred to as the MTS Assay (Promega, Madison, WI). Tissue culture plates were seeded with 5,000 HaCaT cells per well. After overnight incubation, the cells were treated for 24, 48, or 72 h with 200 µL of media containing 1, 5, or 10 µM of each compound (ADJ-310 or PRL-295) per well. Control cells were treated with 10 µL/mL DMSO (1% final concentration) or 250 nM CDDO-Me in media. After treatment, 20 µL of MTS Reagent was added to each well. The plates were then incubated for 30 min at 37 °C. After incubation, the plates were shaken briefly for 5–10 s, after which the absorbance at 490 nm was read using a SpectraMax Plus plate reader (Molecular Devices, San Jose, CA). The results were read and exported using the companion software of the plate reader, SoftMax Pro 7.1 (Molecular Devices), and the statistical analyses were performed using GraphPad Prism 9 (GraphPad Software, San Diego, CA).

Cell migration

In a 6-well plate, 2 brick-shaped silicone molds (Ibidi, Gräfelfing, Germany) with 3 identical openings were each adhered to the bottom of each well, creating 6 identical spaces. HaCaT cells were cultured to confluence within the molds, which were then removed to create 4 identical gaps or in vitro wounds in each well. After the molds were removed, the cells were washed with PBS and then treated with 1 µg/mL mitomycin-C (Sigma Aldrich, St. Louis, MO) for one hour at 37 °C to inhibit proliferation. After mitomycin-C treatment, the cells were washed three times with PBS and then treated with media containing 10 µM each compound (ADJ-310 or PRL-295) or 250 nM of CDDO-Me. Control cells were treated with media containing 10 µL/mL (1% final concentration) DMSO. These in vitro wounds were imaged immediately after mold removal and again every 24 h for three days. Images were processed using ImageJ software (National Institutes of Health, NIH, Bethesda, MD, USA) as described in the "Image Analysis" section below and in the following reference[73]. The rate of migration is expressed as a percentage of the original gap area for each time point.

Oxidative stress

HaCaT cells were cultured as described above until they reached 90–95% confluence. Then, the cells were treated for 24 h with media containing 1 or 10 μM of each compound (ADJ-310 or PRL-295). After treatment, the cells were lysed according to the kit instructions, and the lysates were analyzed using colorimetric detection kits to determine superoxide dismutase (SOD) activity and total glutathione (GSH) content. SOD activity was determined using the Superoxide Dismutase Colorimetric Activity Kit (Invitrogen, Thermo Fisher Scientific), and total GSH content was determined using the Glutathione Colorimetric Detection Kit (Thermo Fisher Scientific). Both kits included detailed instructions and guides that can be viewed online (Thermo Fisher Scientific, catalog numbers EIASODC and EIAGSHC).

Briefly, 2 million cells per sample were lysed by sonication in 500 μL of ice-cold PBS for the SOD assay, and 4.5 million cells per sample were lysed by sonication in a solution of 5% 5-sulfo-salicylic acid (5-SSA) in water for the GSH assay. For the GSH assay, we followed the protocol for detecting total GSH content. Cell lysates at multiple dilutions and the corresponding standards were then mixed with the appropriate reagents and incubated in 96-well plates according to the manufacturer's instructions for each assay. Multiple sample dilutions were included to increase the likelihood that at least one would yield results for all conditions that fell within the reference range for the assay. After incubation, the plates were shaken briefly for 5–10 s, after which the absorbance was read using a SpectraMax Plus plate reader (Molecular Devices) at 450 nm for the SOD assay and 405 nm for the GSH assay. The results were subsequently read and processed, including a best-fit curve, using the plate reader's companion software SoftMax Pro 7.1 (Molecular Devices), with follow-up and confirmation using manual best-fit curve calculations and statistical analyses in GraphPad Prism 9 (GraphPad Software). For the SOD assay, the dilutions yielding the best results were 100% (pure lysate) and 57% lysate in lysis buffer. For the GSH assay, they were 25% and 12.5% lysate in sample diluent. Note that, per the GSH protocol guidelines, dilutions greater than 1:4 are not recommended.

Animal husbandry and experimental design

All husbandry and experimentation procedures were approved by the University of Illinois Chicago Institutional Animal Care and Use Committee under protocol number 19–219. All experiments were performed in accordance with the relevant committee guidelines and regulations, and ARRIVE guidelines were addressed as follows.

For all in vivo experiments, we used 8-week-old female *Lepr*$^{db/db}$ mice (Jackson Labs, strain 000642, Bar Harbor, ME). Mice were allowed to acclimate to their environments for at least one week prior to experimentation. Mice were randomly separated into separate cages upon arrival. Initial cage assignment was done by mouse facility staff, and a randomization sequence was not used. During acclimation, the mice were group-housed (3–5 mice per cage) in standard mouse cages, which were changed weekly. Once the experiments began, the mice were separated and housed in smaller groups (2–3 mice per cage) in large rat cages, and the cages were changed every other day. Larger cages were chosen to allow for more freedom of movement and to reduce the risk of reinjuring wound sites, and the cleaning frequency was increased to reduce the risk of infection and mouse attrition. The facilities were maintained on a 14/10-hour light/dark cycle, and all the animals were given free access to food and water. To minimize the effect of potential confounders, all mice in all groups were housed in the same room and on the same racks within the housing facility. Wounding was done and photos were taken by the same individual throughout the studies to reduce variation. Husbandry was standardized across all groups, and anesthetization, photography, and treatment were done in the same order each day. These studies were not blinded or masked, as the same investigator prepared and administered all treatments, photographed the mice, and performed the analysis.

In these in vivo experiments, the groups being compared were the treatment group(s) receiving either ADJ-310, PRL-295, or CDDO-Me in vehicle solution, and the control group receiving only the vehicle solution of either 40% DMSO in PBS (in the first study) or 25% F-127 Pluronic gel (PG) and 10% DMSO in PBS (in the second study). The experimental unit was a single animal, and the primary outcome measure was wound size. For the first study (vehicle solution: 40% DMSO in PBS), 22 mice were used, with 11 mice allocated to each group. For the second study (vehicle solution: 25% F-127 Pluronic Gel and 10% DMSO in PBS), 24 mice were used, with 6 mice allocated to each group. Across both studies, the total number of mice used was 46. Sample size was determined by exceeding the estimated number of mice predicted to be lost due to attrition such that at least 3 mice remained in each group.

All mice initially included were 7-week-old female *Lepr*$^{db/db}$ diabetic mice (Jackson Labs), which were acclimated for one week prior to experimentation at 8 weeks. There were no additional inclusion criteria. Mice were excluded in the case of premature death, infection, wound convergence or expansion, failure to heal, or wound re-injury due to a cage-mate, self-injury on a housing component, or other unintentional cause. For the first study (vehicle solution: 40% DMSO in PBS), 22 mice were used, and zero mice were excluded, resulting in $n = 11$ for both groups. For the second study (vehicle solution: 25% F-127 Pluronic Gel and 10% DMSO in PBS), 24 mice were used, and 6 mice were excluded according to the criteria described above: one each from the CDDO-Me and PRL-295 groups, and two each from the ADJ-310 and Control groups, resulting in $n = 4$ for the ADJ-310 and Control groups, and $n = 5$ for the CDDO-Me and PRL-295 groups.

In vivo wound healing studies

After acclimation, 8-week-old female *Lepr*$^{db/db}$ mice (Jackson Labs) were separated into larger cages in groups of 2–3, as described above. Mice were anesthetized by isoflurane inhalation, and hair on the dorsum was removed by shaving with electric clippers. After the skin was shaved, it was sanitized using 70% isopropyl alcohol. Then, a dotted line bisecting the dorsum was drawn longitudinally along the spine to mark the center of the back. Anesthesia depth was confirmed by toe-pinching. Then, the dorsal skin was pinched up, folded along the dotted line, and held flat against a sanitized rubber puck. A sterile 8-mm Acu-Punch biopsy punch (Acuderm, Inc., Fort

Lauderdale, FL) was pressed through both layers of the folded skin to create two full-thickness skin wounds, one on either side of the dorsum, separated by the dotted line. Special care was taken to ensure that the wounds were centered between the head and the base of the tail, and the wounds were placed as close as possible to the body of the mouse after dorsal skin folding to reduce the risk of wound expansion, merging, infection, or other complications.

After wounding, the wounds were photographed using a Canon PowerShot ELPH 190-IS digital camera (Canon, USA; Melville, NY) on a fixed tripod with ruler scales affixed to the base to ensure consistent photography. After imaging of the initial wounds, the mice were randomly assigned to groups without the use of a randomization sequence. Then, each wound was treated topically with 30 µL of either a treatment or control (vehicle) solution. Two vehicle solutions were used in these studies: a solution of 40% DMSO in PBS, and a solution of 25% F-127 Pluronic gel (PG) and 10% DMSO in PBS. For the treatment groups, 100 µg of each compound (ADJ-310, PRL-295, or CDDO-Me) was added to 30 µL of the vehicle solution. Treatments were repeated daily beginning on day 0, the day of wounding, until the wounds were closed or no longer visible. Wounds were photographed each day prior to treatment to maximize visibility.

For semi-quantitative real-time PCR analysis of wounds, wounds were treated topically immediately after wounding on D0 and again on D1, for a total of two treatments. Wound tissue was collected 6 h after treatment on D1. To harvest the tissue, mice were euthanized by CO2 inhalation and cervical dislocation, and the wound tissue was collected using a standard punch biopsy instrument and placed in RNALater® (Sigma-Aldrich) and stored at -20ºC. Control mice for the RT-PCR analysis were treated with a solution of 25% F-127 Pluronic gel (PG) and 10% DMSO in PBS.

Real time polymerase chain reaction analysis

For RT-PCR analysis of wound tissue collected 6 h after Day 1 post-wounding treatment, total RNA from 8-mm full thickness skin wounds was extracted using TRIzol (Invitrogen, Waltham, MA). One µg total RNA was then treated with DNase (ThermoFisher Scientific, Waltham, MA) and converted to cDNA using a High-Capacity cDNA Reverse Transcription Kit (Invitrogen). Relative gene expression was determined by semi-quantitative PCR on a StepOnePlus RealTime PCR System (Applied Biosystems, Waltham, MA) using Power SYBR Green PCR Master Mix (Roche, Basel, Switzerland). The $2^{-\Delta\Delta CT}$ method was employed to determine the relative expression of target genes[74]. Figure 8D shows the primers used for our RT-PCR analyses, all of which were from mouse species. Glyceraldehyde-3-phosphate dehydrogenase (*Gapdh*) was used as a reference gene. The DMSO vehicle control group was used as a baseline for comparisons.

Image analysis

Images from both in vitro and in vivo wound healing assays were analyzed using ImageJ software (National Institutes of Health, NIH, Bethesda, MD, USA). For further information about the use of ImageJ, please refer to the following publication[73]. In images that included a known scale measurement, such as the rulers in our mouse wound images, the Straight Line Tool and Set Measurement option was used to set the scale to a known length. If no scale was included, as in the in vitro wound closure images, the area was measured in pixels. Using the Freehand tool, the wound area was manually traced and then quantified using the Measure function. The thickness of each wound was measured 3 times, and the resulting values were averaged to generate a single area measurement for each wound. All the measurements were made in a blinded and randomized fashion. Statistical methods used in the analysis of these measurements are described in detail below, under "Statistical Analysis, Rigor, and Reproducibility."

mRNA sequencing

HaCaT cells were cultured as described above and treated with 250 nM CDDO-Me or 10 µM PRL-295 for 14 h ($n=3$). After treatment, RNA was extracted from the treated cells; RNA sequencing and data analysis, including library preparation, quality control, mapping, quantification, differential gene expression analysis, and enrichment analyses, were conducted by Novogene (Sacramento, CA) using the Illumina NovaSeq 6000 System and PE150 sequencing platform, with paired-end 150-base pair read lengths and more than 20 million read pairs generated per sample. The enrichment pathways analyzed included the Kyoto Encyclopedia of Genes and Genomes (KEGG), Gene Ontology (GO), Human Disease Ontology (DO), and Reactome Pathway Database (Reactome) terms. Further details and reference publications using this technology are available online via Novogene USA. The results are reported using the following nomenclature: HA_C represents control cells treated with media containing DMSO. HA_T1 represents cells treated with CDDO-Me, and HA_T2 represents cells treated with PRL-295. In the figures and legends, additional labels have been added for clarity.

The RNA sequencing data were analyzed by Novogene as described in their "Methods_MedTR" document (Novogene, USA, 2019) and summarized here[75]: Analysis was performed using a combination of programs, including STAR, HTseq, Cufflink and Novogene's wrapped scripts. The alignments were parsed using the TopHat program, and differential expression was determined through DESeq2/edgeR. GO and KEGG enrichment analyses were implemented with ClusterProfiler. Gene fusions and differences in alternative splicing were detected via Star-Fusion and rMATS software. The reference genome and gene model annotation files were downloaded directly from NCBI/UCSC/Ensembl. Indexes of the reference genome were built, and paired-end clean reads were aligned to the reference genome using STAR (v2.5) with the maximal feasible prefix method. HTSeq v0.6.1 was used to count the number of reads mapped to each gene. The FPKM value of each gene was calculated based on the length of the gene and the read count. Differential expression analysis was performed using the DESeq2 R package (2_1.6.3) with a model based on the negative binomial distribution. The resulting P values were adjusted using the Benjamini and Hochberg approach for controlling the false discovery rate (FDR). Genes with an adjusted P value < 0.05 according to DESeq2 were considered to be differentially expressed. To

allow for log adjustment, genes with 0 FPKM were assigned a value of 0.001. Correlations were determined using the cor.test function in R with option set al.ternative = "greater" and method = "Spearman". To identify the correlation between differences, samples were clustered by FPKM using the hierarchical clustering distance method with the heatmap, self-organization mapping, and k-means functions in R. GO enrichment and KEGG pathway analyses were implemented using the clusterProfiler R package, with gene length bias corrected. GO, KEGG, DO, and Reactome terms with corrected p values less than 0.05 were considered to indicate significant enrichment of DEGs. PPI network analysis of the DEGs was performed with the STRING database. Star-fusion (0.8.0) was used to detect fusion genes. rMATS (3.2.1) software was used to analyze the presence of AS events. The results of the Bam alignment for each sample were analyzed using Picard tools (v1.111) and SAMtools (v0.1.18). Single nucleotide polymorphisms were called using HaplotypeCaller in GATK3.4, and ANNOVAR was used to annotate the polymorphisms against the dbSNP database. The TFCat and COSMIC databases were used to annotate the DEGs.

Statistical analysis, rigor, and reproducibility

For quantitative data, statistical analyses were performed using GraphPad Prism 9 software (GraphPad Software). Outliers, if any, were identified among replicates of a single condition using the ROUT Method with Q = 1%. Two-way ANOVA was performed using Tukey and Šidák corrections for multiple comparisons, with a 95% confidence interval and an alpha threshold of 0.05. One-way ANOVA was performed using the Benjamini, Krieger, and Yekutieli two-stage step-up method of correcting for multiple comparisons by controlling the false discovery rate (FDR), with a desired FDR of 0.05. For these one-way ANOVAs, graphed asterisks on pairwise comparisons denote the calculated q values after FDR correction (Figs. 4 and 5). Where applicable, multiplicity-adjusted P values are reported for each comparison. Multiple t tests were performed using the Holm–Šídák method with an alpha threshold of 0.05 (Fig. 3) or the Benjamini–Yekutieli correction method with an FDR of 1% (Fig. 2). Multiple two-tailed unpaired t-testing was performed with Welch's correction (Fig. 8). The area under the curve was calculated with a baseline Y = 0, ignoring all peaks that were less than 10% of the distance from the minimum to the maximum Y.

For all the bar graphs, the error bars represent the standard deviation (SD). Data were expressed as mean ± standard deviation (SD), and their normality was evaluated using the Shapiro-Wilk tests. All experiments were performed in groups of $n = 3$ or greater, where each n represents a biological replicate that may consist of multiple technical replicates (e.g., each mouse is a biological replicate or one n that includes two wounds or technical replicates). In vitro experiments were always conducted in triplicate or greater. For experiments that included multiple dilutions of the same samples, such as the SOD and GSH assays, the results from all dilutions within the reference range were first analyzed together by 2-way ANOVA as described above. Once the best dilution was determined, the results from that dilution were analyzed by one-way ANOVA as described to ensure the accuracy of the reporting. Mice were assigned randomly to groups. Individual measurements were taken in triplicate and averaged to reduce possible variation resulting from manual measurement. For all the treatments, the solutions were freshly prepared immediately prior to use to prevent decay, maximize efficacy, and reduce variability. All analyses were done in a blinded manner.

The authors thank the members of the DiPietro, Moore, and Reddy laboratories. Funding was provided by the following National Institutes of Health grants: F30-DK123989 (Barakat, M), R01-GM50875 (DiPietro, LA), R35-GM139603 (DiPietro, LA), 1R01-AR065941 (Moore, TW), and HL136946 (Reddy, SP), as well as a University of Illinois Chicago Chancellor's Translational Research Initiative (CTRI) Award. We also acknowledge Servier Medical Art by Les Laboratories Servier for their free database of medical art images (available at smart.servier.com) and the Massachusetts Institute of Technology's Whitehead Institute Bioinformatics and Research Computing Venn Diagram Tool (available at http://barc.wi.mit.edu/tools/venn/), which were used in the design of the figures in this publication.

Data availability

In accordance with the Data Sharing Policies of the NIH, the data resulting from this study have been uploaded to a public genomic data repository, the Gene Expression Omnibus, under accession number GSE241267, which can be accessed at: https://www-ncbi-nlm-nih-gov.proxy.cc.uic.edu/geo/query/acc.cgi? acc=GSE241267.

Received: 28 February 2024; Accepted: 8 October 2024
Published online: 24 October 2024

References

1. Naves, C. C. The Diabetic Foot: a historical overview and gaps in current treatment. *Adv. Wound Care (New Rochelle)*. **5**, 191–197 (2016).
2. Barakat, M., DiPietro, L. A. & Chen, L. Limited Treatment options for Diabetic wounds: barriers to clinical translation despite therapeutic success in murine models. *Adv. Wound Care (New Rochelle)*. **10**, 436–460 (2021).
3. Moi, P., Chan, K., Asunis, I., Cao, A. & Kan, Y. W. Isolation of NF-E2-related factor 2 (Nrf2), a NF-E2-like basic leucine zipper transcriptional activator that binds to the tandem NF-E2/AP1 repeat of the beta-globin locus control region. *Proc. Natl. Acad. Sci. U.S.A.***91**, 9926–9930 (1994).
4. He, F., Ru, X. & Wen, T. NRF2, a transcription factor for stress response and Beyond. *Int. J. Mol. Sci.***21, 4777** (2020).
5. Ahmed, S. M., Luo, L., Namani, A., Wang, X. J. & Tang, X. Nrf2 signaling pathway: pivotal roles in inflammation. *Biochim. Biophys. Acta Mol. Basis Dis.***1863**, 585–597 (2017).
6. Malhotra, D. et al. Global mapping of binding sites for Nrf2 identifies novel targets in cell survival response through ChIP-Seq profiling and network analysis. *Nucleic Acids Res.***38**, 5718–5734 (2010).
7. Itoh, K. et al. An Nrf2/Small Maf Heterodimer mediates the induction of phase II detoxifying enzyme genes through antioxidant response elements. *Biochem. Biophys. Res. Commun.***236**, 313–322 (1997).

8. Rouillard, A. D. et al. The harmonizome: a collection of processed datasets gathered to serve and mine knowledge about genes and proteins. *Database*. baw100 (2016). (2016).
9. Martens, M. et al. WikiPathways: connecting communities. *Nucleic Acids Res.***49**, D613–D621 (2021).
10. Campbell, M. R. et al. Novel Hematopoietic Target Genes in the NRF2-Mediated Transcriptional Pathway. *Oxidative Medicine and Cellular Longevity*. 120305 (2013). (2013).
11. Hayes, J. D. & Dinkova-Kostova, A. T. The Nrf2 regulatory network provides an interface between redox and intermediary metabolism. *Trends Biochem. Sci.***39**, 199–218 (2014).
12. Hirotsu, Y. et al. Nrf2-MafG heterodimers contribute globally to antioxidant and metabolic networks. *Nucleic Acids Res.***40**, 10228–10239 (2012).
13. Lee, J. M. et al. Nrf2, a multi-organ protector? *FASEB J.***19**, 1061–1066 (2005).
14. Namani, A. et al. Genome-wide global identification of NRF2 binding sites in A549 non-small cell lung cancer cells by ChIP-Seq reveals NRF2 regulation of genes involved in focal adhesion pathways. *Aging (Albany NY)*. **11**, 12600–12623 (2019).
15. Jung, K. A. et al. Identification of aldo-keto reductases as NRF2-target marker genes in human cells. *Toxicol. Lett.***218**, 39–49 (2013).
16. Penning, T. M. Aldo-Keto reductase regulation by the Nrf2 system: implications for stress response, Chemotherapy Drug Resistance, and carcinogenesis. *Chem. Res. Toxicol.***30**, 162–176 (2017).
17. Alam, J. et al. Nrf2, a Cap'n'Collar transcription factor, regulates induction of the heme oxygenase-1 gene. *J. Biol. Chem.***274**, 26071–26078 (1999).
18. Braun, S. et al. Nrf2 transcription factor, a novel target of keratinocyte growth factor action which regulates gene expression and inflammation in the healing skin wound. *Mol. Cell. Biol.***22**, 5492–5505 (2002).
19. Chan, K. & Kan, Y. W. Nrf2 is essential for protection against acute pulmonary injury in mice. *Proc. Natl. Acad. Sci. U.S.A.***96**, 12731–12736 (1999).
20. Dodson, M., Castro-Portuguez, R. & Zhang, D. D. NRF2 plays a critical role in mitigating lipid peroxidation and ferroptosis. *Redox Biol.***23**, 101107 (2019).
21. He, F., Antonucci, L. & Karin, M. NRF2 as a regulator of cell metabolism and inflammation in cancer. *Carcinogenesis*. **41**, 405–416 (2020).
22. Jiang, C. et al. Nrf2/ARE is a key pathway for curcumin-mediated protection of TMJ chondrocytes from oxidative stress and inflammation. *Cell. Stress Chaperones*. **25**, 395–406 (2020).
23. Motohashi, H. & Yamamoto, M. Nrf2–Keap1 defines a physiologically important stress response mechanism. *Trends Mol. Med.***10**, 549–557 (2004).
24. Piantadosi, C. A., Carraway, M. S., Babiker, A. & Suliman, H. B. Heme oxygenase-1 regulates cardiac mitochondrial biogenesis via Nrf2-mediated transcriptional control of nuclear respiratory factor-1. *Circ. Res.***103**, 1232–1240 (2008).
25. Rangasamy, T. et al. Genetic ablation of Nrf2 enhances susceptibility to cigarette smoke-induced emphysema in mice. *J. Clin. Investig.***114**, 1248–1259 (2004).
26. Saha, S., Buttari, B., Panieri, E., Profumo, E. & Saso, L. An overview of Nrf2 Signaling Pathway and its role in inflammation. *Molecules***25**, 5474 (2020).
27. Venugopal, R. & Jaiswal, A. K. Nrf1 and Nrf2 positively and c-Fos and Fra1 negatively regulate the human antioxidant response element-mediated expression of NAD(P)H:quinone oxidoreductase1 gene. *Proc. Natl. Acad. Sci. U.S.A.***93**, 14960–14965 (1996).
28. Cuadrado, A. et al. Therapeutic targeting of the NRF2 and KEAP1 partnership in chronic diseases. *Nat. Rev. Drug Discov*. **18**, 295–317 (2019).
29. Liby, K. T. & Sporn, M. B. Synthetic oleanane triterpenoids: multifunctional drugs with a broad range of applications for prevention and treatment of chronic disease. *Pharmacol. Rev.***64**, 972–1003 (2012).
30. de la Rojo, M., Chapman, E. & Zhang, D. D. NRF2 and the hallmarks of Cancer. *Cancer Cell.***34**, 21–43 (2018).
31. Dinkova-Kostova, A. T. & Copple, I. M. Advances and challenges in therapeutic targeting of NRF2. *Trends Pharmacol. Sci.***44**, 137–149 (2023).
32. Long, M. et al. An essential role of NRF2 in Diabetic Wound Healing. *Diabetes*. **65**, 780–793 (2016).
33. Lee, Y. J. et al. Increased protein oxidation and decreased expression of nuclear factor E2-related factor 2 protein in skin tissue of patients with diabetes. *Clin. Exp. Dermatol.***40**, 192–200 (2015).
34. David, J. A., Rifkin, W. J., Rabbani, P. S. & Ceradini, D. J. The Nrf2/Keap1/ARE Pathway and Oxidative Stress as a Therapeutic Target in Type II Diabetes Mellitus. *J Diabetes Res*. 4826724 (2017). (2017).
35. Rabbani, P. S. et al. Targeted Nrf2 activation therapy with RTA 408 enhances regenerative capacity of diabetic wounds. *Diabetes Res. Clin. Pract.***139**, 11–23 (2018).
36. Li, M. et al. Nrf2 suppression delays Diabetic Wound Healing through sustained oxidative stress and inflammation. *Front. Pharmacol.***10**, 1099 (2019).
37. Cai, F., Chen, W., Zhao, R. & Liu, Y. Mechanisms of Nrf2 and NF-kappaB pathways in diabetic wound and potential treatment strategies. *Mol. Biol. Rep.* 50, 5355-5367 (2023).
38. Victor, P., Sarada, D. & Ramkumar, K. M. Pharmacological activation of Nrf2 promotes wound healing. *Eur. J. Pharmacol.***886**, 173395 (2020).
39. Jindam, A., Yerra, V. G. & Kumar, A. Nrf2: a promising trove for diabetic wound healing. *Ann. Transl Med.***5**, 469 (2017).
40. Rampin, A. et al. Recent advances in KEAP1/NRF2-Targeting strategies by Phytochemical Antioxidants, nanoparticles, and Biocompatible scaffolds for the treatment of Diabetic Cardiovascular complications. *Antioxid. Redox Signal.***36**, 707–728 (2022).
41. Robledinos-Antón, N., Fernández-Ginés, R., Manda, G. & Cuadrado, A. Activators and Inhibitors of NRF2: A Review of Their Potential for Clinical Development. *Oxid Med Cell Longev*. 9372182 (2019). (2019).
42. Yagishita, Y., Gatbonton-Schwager, T. N., McCallum, M. L. & Kensler, T. W. Current Landscape of NRF2 biomarkers in clinical trials. *Antioxid. (Basel)* 9, 716 (2020).
43. Sporn, M. B. et al. New synthetic triterpenoids: potent agents for prevention and treatment of tissue injury caused by inflammatory and oxidative stress. *J. Nat. Prod.***74**, 537–545 (2011).
44. Cakir, I. et al. Sulforaphane reduces obesity by reversing leptin resistance. *Elife***11**, e67368 (2022).
45. Saha, P. K., Reddy, V. T., Konopleva, M., Andreeff, M. & Chan, L. The triterpenoid 2-cyano-3,12-dioxooleana-1,9-dien-28-oic-acid methyl ester has potent anti-diabetic effects in diet-induced diabetic mice and lepr(db/db) mice. *J. Biol. Chem.***285**, 40581–40592 (2010).
46. Sun, Q. et al. Bardoxolone and bardoxolone methyl, two Nrf2 activators in clinical trials, inhibit SARS-CoV-2 replication and its 3 C-like protease. *Signal. Transduct. Target. Therapy*. **6**, 212 (2021).
47. Cuadrado, A. et al. Can activation of NRF2 be a strategy against COVID-19? *Trends Pharmacol. Sci.***41**, 598–610 (2020).
48. Itoh, K., Ishii, T., Wakabayashi, N. & Yamamoto, M. Regulatory mechanisms of cellular response to oxidative stress. *Free Radic Res.***31**, 319–324 (1999).
49. Itoh, K. et al. Keap1 represses nuclear activation of antioxidant responsive elements by Nrf2 through binding to the amino-terminal Neh2 domain. *Genes Dev.***13**, 76–86 (1999).
50. Horie, Y. et al. Molecular basis for the disruption of Keap1-Nrf2 interaction via Hinge & Latch mechanism. *Commun. Biol.***4**, 576 (2021).
51. Clulow, J. A. et al. Competition-based, quantitative chemical proteomics in breast cancer cells identifies new target profiles for sulforaphane. *Chem. Commun. (Camb)*. **53**, 5182–5185 (2017).

52. Liu, P. et al. Non-covalent NRF2 activation confers Greater Cellular Protection than Covalent Activation. *Cell. Chem. Biol.***26**, 1427–1435e1425 (2019).
53. Yore, M. M., Kettenbach, A. N., Sporn, M. B., Gerber, S. A. & Liby, K. T. Proteomic analysis shows synthetic oleanane triterpenoid binds to mTOR. *PloS One*. **6**, e22862 (2011).
54. Richardson, B. G. et al. Replacement of a Naphthalene Scaffold in Kelch-like ECH-Associated protein 1 (KEAP1)/Nuclear factor (erythroid-derived 2)-like 2 (NRF2) inhibitors. *J. Med. Chem.***61**, 8029–8047 (2018).
55. Richardson, B. G., Jain, A. D., Speltz, T. E. & Moore, T. W. Non-electrophilic modulators of the canonical Keap1/Nrf2 pathway. *Bioorg. Med. Chem. Lett.***25**, 2261–2268 (2015).
56. Dayalan Naidu S. et al. The isoquinoline PRL-295 increases the thermostability of Keap1 and disrupts its interaction with Nrf2. *iScience*. **25**, 103703 (2022).
57. Barbieri, J. S., Wanat, K. & Seykora, J. in *In Pathobiology of Human Disease*. 1134–1144 (eds Linda, M., McManus & Mitchell, R. N.) (Academic, 2014).
58. Dinkova-Kostova, A. T. et al. Extremely potent triterpenoid inducers of the phase 2 response: correlations of protection against oxidant and inflammatory stress. *Proc. Natl. Acad. Sci. U.S.A.***102**, 4584–4589 (2005).
59. Wang, Y. Y., Yang, Y. X., Zhe, H., He, Z. X. & Zhou, S. F. Bardoxolone methyl (CDDO-Me) as a therapeutic agent: an update on its pharmacokinetic and pharmacodynamic properties. *Drug Des. Devel Ther.***8**, 2075–2088 (2014).
60. Kanehisa, M. Toward understanding the origin and evolution of cellular organisms. *Protein Sci.***28**, 1947–1951 (2019).
61. Kanehisa, M., Furumichi, M., Sato, Y., Kawashima, M. & Ishiguro-Watanabe M. KEGG for taxonomy-based analysis of pathways and genomes. *Nucleic Acids Res.***51**, D587–D592 (2023).
62. Kanehisa, M. & Goto, S. KEGG: kyoto encyclopedia of genes and genomes. *Nucleic Acids Res.***28**, 27–30 (2000).
63. Revathidevi, S. & Munirajan, A. K. Akt in cancer: Mediator and more. *Semin Cancer Biol.***59**, 80–91 (2019).
64. Wang, Z. ErbB receptors and Cancer. *Methods Mol. Biology (Clifton N J)*. **1652**, 3–35 (2017).
65. Zhang, C. et al. Gain-of-function mutant p53 in cancer progression and therapy. *J. Mol. Cell. Biol.***12**, 674–687 (2020).
66. Sheehan, P., Jones, P., Caselli, A., Giurini, J. M. & Veves, A. Percent change in wound area of diabetic foot ulcers over a 4-week period is a robust predictor of complete healing in a 12-week prospective trial. *Diabetes Care*. **26**, 1879–1882 (2003).
67. Probst, B. L. et al. RTA 408, a Novel Synthetic Triterpenoid with Broad Anticancer and anti-inflammatory activity. *PloS One*. **10**, e0122942 (2015).
68. Lazzara, P. R. et al. Isoquinoline Kelch-like ECH-Associated protein 1-Nuclear factor (erythroid-Derived 2)-like 2 (KEAP1-NRF2) inhibitors with High Metabolic Stability. *J. Med. Chem.***63**, 6547–6560 (2020).
69. Wu, S., Lu, H. & Bai, Y. Nrf2 in cancers: a double-edged sword. *Cancer Med.***8**, 2252–2267 (2019).
70. Hamblet, C. et al. Transcriptional dynamics of NRF2 overexpression and KEAP1-NRF2 inhibitors in human cell line and primary lung cells. *Antioxid. (Basel)* 13, 924 (2024).
71. Jain, A. D. et al. Probing the structural requirements of non-electrophilic naphthalene-based Nrf2 activators. *Eur. J. Med. Chem.***103**, 252–268 (2015).
72. Lazzara, P. R. et al. Synthesis and evaluation of Noncovalent Naphthalene-based KEAP1-NRF2 inhibitors. *ACS Med. Chem. Lett.***11**, 521–527 (2020).
73. Schneider, C. A., Rasband, W. S. & Eliceiri, K. W. NIH image to ImageJ: 25 years of image analysis. *Nat. Methods*. **9**, 671–675 (2012).
74. Livak, K. J. & Schmittgen, T. D. Analysis of relative gene expression data using real-time quantitative PCR and the 2(-Delta Delta C(T)) method. *Methods*. **25**, 402–408 (2001).
75. Novogene. Methods_MedTR. Novogene USA, methods description provided as part of the mRNA sequencing analysis and results report, (2019).

Acknowledgements

The authors thank the members of the DiPietro, Moore, and Reddy laboratories. Funding was provided by the following National Institutes of Health grants: F30-DK123989 (Barakat, M), R01-GM50875 (DiPietro, LA), R35-GM139603 (DiPietro, LA), 1R01-AR065941 (Moore, TW), and HL136946 (Reddy, SP), and by a UIC Chancellors Translational Research Initiative Award (Moore, TW; DiPietro LA). We also acknowledge Servier Medical Art by Les Laboratories Servier for their free database of medical art images (available at smart.servier.com) and the Massachusetts Institute of Technology's Whitehead Institute Bioinformatics and Research Computing Venn Diagram Tool (available at http://barc.wi.mit.edu/tools/venn/), which were used in the design of the figures in this publication.

Author contributions

Author contributions are reported here using Contributor Roles Taxonomy (CRediT). For each CRediT category, the authors are listed using their initials in the order they appear in the list of authors. Conceptualization: MB, BPD, TWM, and LAD. Methodology: MB, CH, LC, BPD, JS, KJS, TJ, TWM, and LAD. Validation: MB, LC, TWM, and LAD. Formal analysis: MB, CH. Investigation: MB, CH, LC, BPD, JS, AX, RW, AA, SPR, TWM, and LAD. Resources: MB, LC, JS, KJS, TJ, AA, SPR, TWM, and LAD. Data curation: MB, CH, LC, AA, SPR, TWM, and LAD. Writing – original draft: MB. Writing – review and editing: MB, LC, TWM, and LAD. Visualization: MB, CH, KJS, TWM, and LAD. Supervision: LC, TWM, and LAD. Project administration: MB, TWM, and LAD. Funding acquisition: MB, SPR, TWM, and LAD.

Funding

Funding Acquistion: MB, SPR, TWM, and LAD.

Declarations

Competing interests

The authors declare no competing interests.

Author disclosure and competing interests

The authors have no competing financial interests or other conflicts of interest to disclose. The content of this article was expressly written by the authors listed, and no ghostwriters were used.

Additional information

Correspondence and requests for materials should be addressed to T.W.M. or L.A.D.